Metallographic Study of Gamma – Gamma Prime Structure in the Ni-based Superalloy GTD111

by

Apostolos Kountras

B.S. Aeronautical/Mechanical Engineering, Hellenic Air Force Academy, 1991
MBA, National Technical University of Athens, Greece, 2003

Submitted to the Department of Material Science and Engineering
in Partial Fulfillment of the Requirements for the Degree of
Master of Science in Materials Science and Engineering

at the

Massachusetts Institute of Technology

June 2004

Signature of Author.....
Department of Material Science and Engineering
April 27, 2004

Certified by .....
Thomas W. Eagar
Thomas Lord Professor of Materials Engineering and Engineering Systems
Thesis Supervisor

Accepted by .....
Carl V. Thompson II
Stavros Salapatas Professor of Materials Science and Engineering
Chair, Departmental Committee on Graduate Students

Metallographic Study of Gamma – Gamma Prime Structure in the Ni-based Superalloy GTD111

by

Apostolos Kountras

Submitted to the Department of Materials Science and Engineering
on April 27, 2004, in Partial Fulfillment of the
Requirements for the Degree of
Master of Science in Materials Science and Engineering

Abstract

The potential for land-based turbine buckets material rejuvenation presents a significant commercial and scientific interest. Ni-based superalloy GTD111 is used at a number of GE-manufactured power generation turbines. The outstanding creep resistance features of Ni-based superalloys can be attributed to a large extent, to the gamma prime (γ') precipitates found within the FCC γ-matrix. Service-induced material degradation mainly involves coarsening and shape transformation of γ'-phase precipitates; therefore, any bucket repair attempt should primarily address the restoration of γ' precipitates to the original configuration.

In the present study a quantitative metallographic analysis of GTD111 alloy under different conditions was performed. Several micrographs were taken and analysed using image analysis software. Gamma prime precipitate size was measured and compared between the different alloy conditions, leading to useful conclusions concerning material degradation as a result of high-temperature service exposure. In addition, microstructural transformations observed as a result of different heat treatments, formed the basis for investigation of procedures that can potentially restore the alloy microstructure in the original condition. High temperature solution and aging heat treatments sequence is considered as potentially sufficient for restoring the GTD111 microstructure.

Finally, the measurements were examined for correlation with existing γ' particle coarsening theory, by calculating and evaluating the metal service temperature during service. A satisfactory correlation exists.

Thesis Supervisor: Thomas W. Eagar
Title: Thomas Lord Professor of Materials Engineering and Engineering Systems

Table of Contents

List of Illustrations and Figures

List of Tables

Acknowledgements

I would like to thank all the people who worked with and helped me on this thesis. Without their support the completion of this project would have been extremely difficult if not impossible. First, I would like to thank Professor Thomas W. Eagar for providing invaluable guidance through his deep knowledge on metallurgy and unique leadership skills. My working under his supervision was a real learning experience in multiple ways. Certainly, I feel indebted to Mr. Richard Fenton and Dr. Zengmei Wang Koenigsmann of *Chromalloy New York, Co.* for their support to this project both in terms of material samples preparation and provision but also of advise and technical expertise guidance.

I would like to also thank Ms. Jerilyn Hill for her considerable help in various administrative issues, and Mr. Donald Galler in DMSE Welding Lab for teaching and assisting me in the usage of Scanning Electron Microscope.

Last and certainly not least, I would like to thank my wife Evanthoula and our children Vasiliki and Theofani for their tolerance and strong support not only in the accomplishment of this project but throughout my whole long-lasting educational effort.

1. Introduction

Turbine engine industry economics have changed significantly in the last decade; improved engine reliability has led to increased inspection intervals, whilst the high level of competition has drastically diminished the profitability margins for the engine manufacturers. It is commonly accepted that new engine acquisition contracts serve more as ways to secure long lasting profitable support contracts in the future, rather than as profit sources themselves. It is suggested that the engine manufacturers, confined by the intense competition, reach new sales agreements solely based on the revenues expected later on, during the operation and product support phase of the programs.

Operation and maintenance costs generally constitute a significant part of turbine engine life-cycle cost. This is particularly true in the case of power generation land-based turbine engines, where the engine parts replacements account for more than one third of the maintenance cost [1]. As a result, there is significant pressure for parts replacement and from the engine operators' perspective, a particular interest for repair and rejuvenation of engine parts in order to minimize parts replacement costs. In the case of land-based gas turbines there is a high interest in the development of rejuvenation/repair procedures of engine turbine blades (buckets) since replacement part prices are on the order of a few thousands of dollars.

The polycrystalline Ni-based superalloy GTD111, developed by General Electric (GE) is extensively used for high-temperature operating buckets. It should be noted that all GE Frame 7 (MS7000 series) engines stage 1 and 2 buckets, as well as several up-rated Frame 3, 5, and 9 engine model buckets are manufactured using GTD111 material [2], [3]. Based on data as of 1995 [2], more than 540 MS7000 series engines are operating around the world, and the number of engines using GTD111 made buckets is even higher when taking into account Frame 3, 5, and 9 series engines.

The equiaxed version of GTD111 entered service in 1984, and directionally solidified (DS) GTD111 was introduced in the late 80's [3]. The service life of a large number of GTD111 buckets has far exceeded 60000 hours reaching the inspection/condemnation cycle. Therefore, GTD111 rejuvenation/repair development and bucket service life extension becomes even more critical and has significant commercial interest.

To date there is limited published data pertaining to the metallurgical and mechanical properties of the GTD111 alloy, as well as relevant rejuvenation/repair procedures. It is known that the microstructure of alloy GTD111 degrades when exposed to long-term high-temperature operation, with subsequent negative effects on the alloy mechanical properties. Therefore, rejuvenation of the microstructure and recovery of the original material microstructural features and mechanical properties should be part of the bucket repair process.

The present research project was accomplished in the context of such an effort for the development of repair procedures for GTD111(DS) engine run buckets. It is known that material degradation partially refers to the changes of γ'-phase precipitates size and shape as a result of long-term and high-temperature exposure. Therefore, the main objective of the project was to perform a quantified metallographic study of the $\gamma - \gamma$' structure as observed in different GTD111(DS) alloy conditions.

2. Experimental Program

The intent of the experimental part of the project was to characterize the morphology (size and shape) of gamma prime (γ') precipitates in the GTD111(DS) microstructure, as well as to observe the grain boundary features of the microstructure. The material was studied under six (6) different conditions:

a. Original.
b. After service.
c. Aged.
d. After Hot Isostatic Pressure (HIP) treatment.
e. HIPed and then aged.
f. HIPed, solutionized and then aged.

2.1 Material Samples

For all alloy condition categories, Chromalloy New York (CNY) company provided a total of 64 samples extracted from two in-service Frame 7FA stage 2 buckets: serial numbers (S/N) CIUM102849 (36000 hours operating time) and CIUM102083 (38000 hours operating time), hereafter referred to as S/N 849 and 083 respectively. Figure 1 depicts bucket S/N CIUM102849.

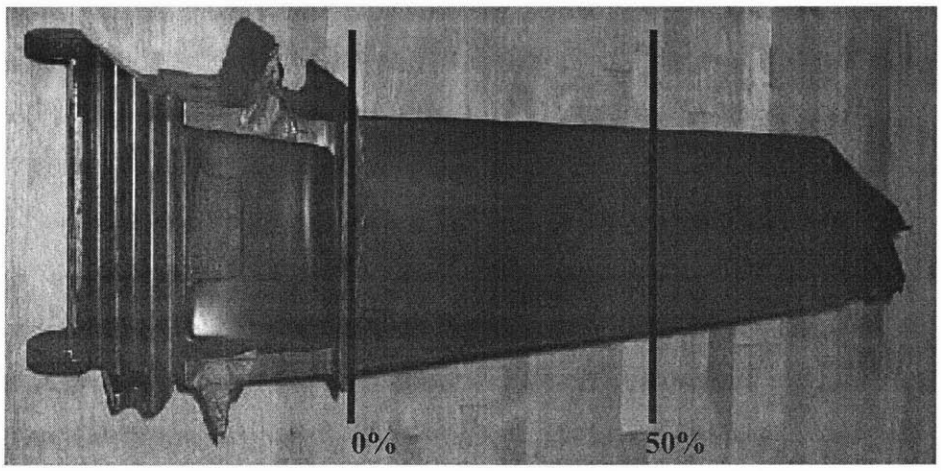

Figure 1 - Frame 7FA stage 2 bucket

The samples were manufactured out of material from 0%, 25% and 50% blade span locations and their chord-wise positions varied from 10% to 60% of bucket chord length. Half of the samples were taken from transverse planes (normal to the span-wise direction of bucket solidification) and half were taken from longitudinal planes (parallel to the bucket span-wise direction). All of them were cut and prepared by CNY personnel. In order to expose the different phases of interest to the Scanning Electron Microscope (SEM) observation, the samples were chemically etched with AG-21 etchant (lactic etch consisting of 61% lactic acid, 36% nitric acid, and 3% HF).

2.2 Material Condition Categories

a. "Original" Material: Samples taken from the root sections of the buckets were considered as sufficiently representing material in the "as-manufactured" condition. The operating metal temperature at this location is relatively low and, as a result, the base metal is assumed to have similar microstructure with the original GTD111(DS) material of the buckets at the beginning of their operational life. A total number of sixteen (16) samples were taken from the root sections of both buckets. The objective of the analysis of the material in the original condition was to take measurements of the γ' precipitates in the as-manufactured condition, and prior to any service-induced degradation. In addition, it was desirable to depict the morphology of grain boundaries, for comparison purposes with the respective configuration of the alloy under different conditions, and specifically after heat treatments aiming at rejuvenation of the microstructure.

b. "After Service" Material: Totally sixteen (16) samples were taken from the 0%, 25% and 50% span locations of the two buckets (eight from each one of them). Only the service time of each bucket was known, as mentioned previously, while the significant operating parameter of metal operating temperature was not. These samples were used in order to identify and quantify the effects of service exposure to bucket microstructure. In particular, more attention was paid to the changes imposed to the shape and size of γ' precipitates as well as to the grain boundary morphology.

c. Aged Material: Sixteen (16) samples equally selected from both buckets have undergone aging heat treatment at CNY (1550° F for 24 hours). Again, the features of interest in the metallographic examination, were the γ' precipitates and the morphology of grain boundaries. At this point it should be mentioned that in order to alleviate any measurement deviations induced by bucket-to-bucket variability, the material condition categories (a), (b) above and (c), were further divided according to bucket S/N. Thus, it was possible to draw more sound conclusions on the effects of service exposure to the original material, and of aging heat treatment to the after-service material.

d. HIPed Material: Eight (8) samples from both buckets have undergone Hot Isostatic Pressure (HIP) treatment (15 Ksi at 2200° F for 4 hours) with no other heat treatment following. The samples of this and the two following categories (which also involve HIPed samples) were not further divided to S/N sub-categories because the number of samples per S/N was small. Further decrease of sample size as a result of sub-categories split would increase the statistical variance of the measurements. In addition, the HIP process that was applied to the samples of the three categories caused extensive changes in material microstructure and essentially eliminated all S/N-bucket microstructure differences.

e. HIPed – Aged Material: Four samples from both buckets that had previously undergone HIP treatment were further aged at 1550° F for 24 hours.

f. HIPed – Solutionized – Aged Material: After being HIP treated, four samples (from both buckets) received a solution heat treatment (2150° F for 2 hours and 2050° F for 2 hours) and a final aging heat treatment (1550° F for 24 hours). The selection of this particular heat treatment sequence was based on previous work [4], which showed that it generated GTD111 alloy microstructure with good stress rupture properties.

2.3 Microscopic Analysis

All 64 samples were analysed in the LEO VP-438 Scanning Electron Microscope (SEM) of Materials Science and Engineering Department of MIT. The microscope is

regularly calibrated as detailed in Appendix A. The analysis mostly involved the examination of the alloy microstructure in the dendritic region, at 1,000X, 2,500X, and 10,000X magnifications. In the cases where the size of features of interest was small and did not allow for enough accuracy in dimensional measurements, higher magnification was used (usually 20,000X but in extreme cases even 100,000X). An average number of 15 micrographs per sample were taken for further analysis. Since one of the objectives of the project was to take dimensional measurements of γ' precipitates, it was desirable to have enough micrographs per sample in order to minimize the statistical variance of the measurements.

As mentioned previously, the microstructure region of interest was the dendritic region, where the typical $\gamma - \gamma$' structure of superalloys is developed. In addition, particular attention was paid to the grain boundaries where microstructural changes take place as a result of service degradation and alloy heat treatments.

2.4 Micrographs Analysis

The analysis of grain boundary regions mainly involved the identification of the existing intergranular phases and the description of their morphology. No quantitative analysis was made in the grain boundary phases. For the $\gamma - \gamma$' structure within the grains it was deemed appropriate to measure the γ' phase volume fraction and dimensions of the γ' particles.

For accomplishment of measurements, the free software *Scion Image for Windows* of Scion Co[1] was used. *Scion Image* gave the capability for direct measurements out of the micrographs and export of the large amount of data to separate electronic files for further statistical processing. An average of approximately three micrographs from each sample was analyzed, totaling 196 analyzed micrographs. Figure 2 is an example of an SEM micrograph that was further processed using *Scion Image* software (Figure 3).

[1] http://www.scioncorp.com

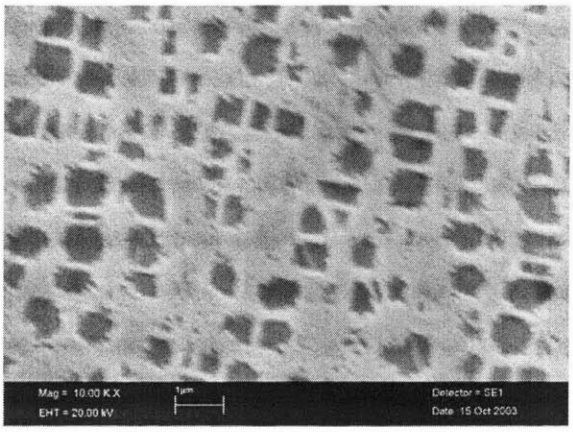

Figure 2 - SEM micrograph

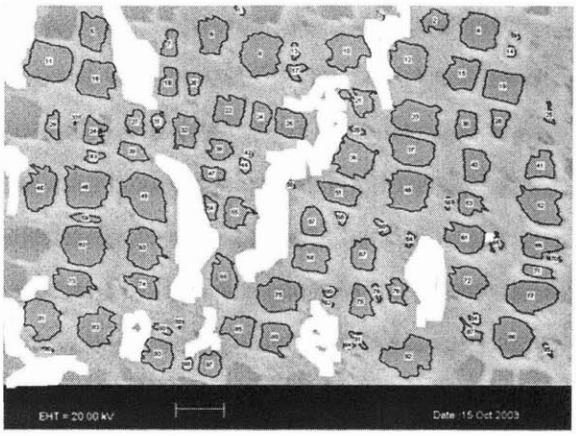

Figure 3 - *Scion Image* processed micrograph

In order to calculate the γ' volume fraction for each sample, the γ' particle area fraction was measured in each micrograph of the particular sample, as the percentage of micrograph area covered by γ' precipitates. Subsequently, the average γ' area fraction over the total number of micrographs was calculated. As detailed in [5] the average γ' phase area fraction is equal to the γ' volume fraction.

The γ' particles dimensional measurements performed were the following:

a. Particle area (in μm^2).
b. Major particle dimension (in μm).
c. Minor particle dimension (in μm).

In order to allow for the γ' precipitates size characterization and comparisons between the different alloy condition categories, the particle area measurement was used to calculate the radius of a hypothetical sphere with equal volume to the particle. All further calculations and comparisons were made using the equivalent-sphere radius dimension, based on the fact that all particle coarsening theories and formulas found in the literature refer to spherical particles.

Since the most prevalent particle shape was the cuboidal with various degrees of roundness, it was assumed that the particle was cubic, with the micrograph plane cutout being normal to one of the three symmetry axis of the cube. Thus, for particle volume (V_p), measured particle cutout area (A_p), and radius of equal volume sphere (R), we have:

$$V_p = (A_p)^{\frac{3}{2}} = \frac{4 \cdot \pi}{3} \cdot R^3 \qquad \text{and thus,} \quad R = \left(\frac{3}{4 \cdot \pi}\right)^{\frac{1}{3}} \cdot (A_p)^{\frac{1}{2}} \tag{1}$$

3. Description of GTD111 Alloy

General Electric developed in 1980s the Ni-based superalloy GTD111 for application in engine turbines. Published data [3] show that the equiaxed version of GTD111 has an approximate increase of 20°C in creep rupture over the up-to-then industry standard superalloy IN-738. The directionally solidified version of GTD111 compared to the equiaxed version has an improved creep life, impact stress (by more than 33%), and thermal-fatigue resistance (by more than ten times) [3].

3.1 Composition

The nominal chemical composition of the GTD111 alloy [3] is presented in Table 1. In addition, during previous quantitative chemical analysis [6] the per weight chemical composition was measured, and based on the René 80 tolerances, the minimum/maximum limits for every element were calculated (see Table 1).

	C	B	Cr	Co	Ni	Mo	W	Ta	Al	Ti	Zr	Hf
Nominal	0.1	0.01	14	9.5	BALANCE	1.5	3.8	2.8	3.0	4.9	-	-
Measured	0.103	0.015	13.78	9.21		1.54	3.7	2.88	3.02	4.81	0.01	0.04
Estimated Maximum	0.12	0.02	14.3	10.0		1.7	4.1	3.1	3.2	5.1	0.08	0.08
Estimated Minimum	0.08	0.01	13.7	9.0		1.3	3.5	2.5	2.8	4.7	0.02	0.02

Table 1 - GTD111 chemical composition

The above elements could be organized in the following three classes [7]:

a. Elements that prefer and form the face-centred-cubic (FCC) austenitic γ base matrix. These are elements from V, VI, and VII Periodic Table Groups and include Ni, Co, Cr, Mo, and W.

b. Elements that make up the γ' precipitates of general type Ni_3X. These are from Groups III, IV, and V and include Al, Ti, Ta, and Hf.

c. B, C, and Zr form a third class of elements, which tend to segregate at grain boundaries.

In addition to the classification above, the elements found in GTD111 can also be identified as carbide-forming (Cr, Mo, W, Ta, and Ti) and oxide-forming elements (Cr and Al), which develop adherent diffusion-resistant oxides that protect the alloys from the environment [7].

3.2 Alloy Microstructure

The microstructural features of the alloy that were observed in the "original" material samples were similar to other Ni-based superalloys, as described in the literature [7]. They are as follows:

Gamma Phase (γ): It is the continuous basic matrix that can be seen in Figure 4. It is an FCC Ni-based austenitic phase that contains a high percentage of solid-solution elements such as Co, Cr, Mo, and W. Although pure Ni is not characterized by exceptionally high modulus of elasticity or low diffusivity (these are two factors that improve creep rupture resistance), the γ matrix is widely used in the high-temperature, adverse environment of gas turbines. The GTD111 alloy, as well as some of the rest of Ni-based alloys, is used at temperatures higher than even 80% of the melting temperature ($0.8xT_{melting}$) with remarkable creep rupture resistance performance. According to Sims et al [7], the basic reasons for this endurance can be attributed to the following factors:

a. High tolerance of Ni for alloying with relative phase stability.
b. With Cr added, there is a tendency to form Cr_2O_3-rich protective areas that inhibit the diffusion of metallic elements outward and of O, N, and other aggressive atmospheric elements inward.
c. Tendency at high temperatures to form Al_2O_3-rich areas with exceptional resistance to oxidation.

Additionally, it is known [7] that the γ-matrix increased strength is achieved via solid solution strengthening mechanism, with Co, Cr, Mo, W, Ti, and Al being the solute elements.

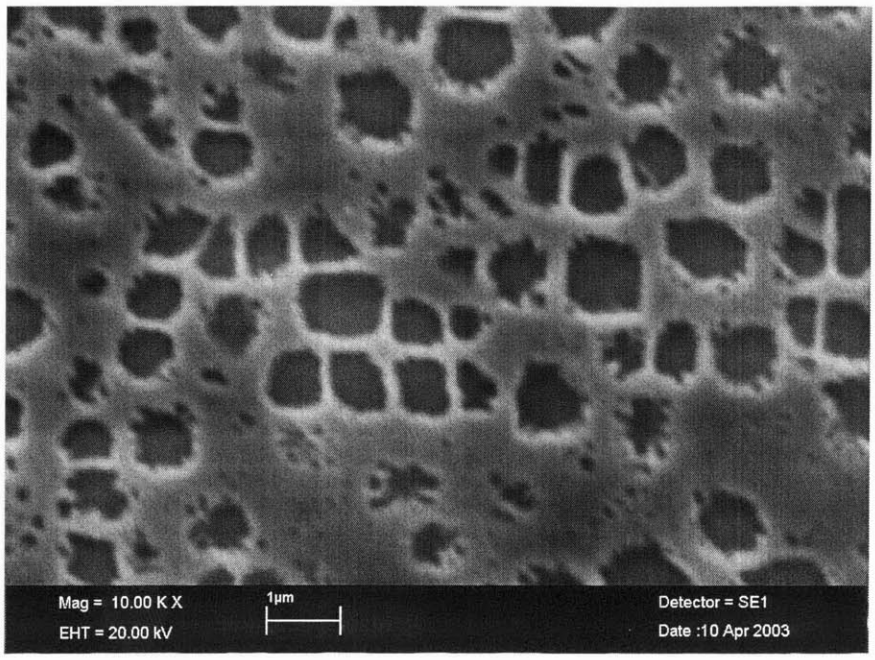

Figure 4 - GTD111 γ - γ' structure

Gamma Prime Phase (γ'): High-nickel matrix favors the precipitation of FCC A_3B type intermetallic compound, the γ' phase. It is homogeneously nucleated as a result of the compatibility of γ' FCC crystal lattice constant with γ matrix lattice parameter (approximately 0.1-0.5% mismatch). Therefore, it has low surface energy and remarkable long-time stability.

The γ'-precipitates in the GTD111 alloy are of the type $Ni_3(Al,Ti)$ and in the original material condition they were observed evenly distributed in the γ matrix, in two shapes/sizes (Figure 4):

a. Primary γ' precipitates, with cuboidal shape and an average size of 0.54μm.
b. Secondary γ' precipitates, with spherical shape and an average size of 0.1μm.

The formation of γ′ precipitate is a rather fortunate phenomenon that has a major contribution to the strength of γ-γ′ GTD111 DS alloy. Briefly, it can be said that the outstanding alloy strengthening is achieved by dislocation interactions; dislocations are forced to cut or by-pass the γ' precipitates.

The properties of γ′-strengthened alloys are quite dependent upon factors such as:

i. Volume fraction of γ′.
ii. Size of γ′ precipitates.
iii. Solid solution strengthening parameters of both γ and γ′ phases, and

iv. Presence of hyperfine (secondary) γ'. Such secondary γ' precipitates can be noticed in Figure 4.

Furthermore, the inherent ductility of γ' prevents it from being brittle and initiating material fracture. Unfortunately, this is a completely different behaviour to the one encountered by the formation of Topologically Close Packed (TCP) phases. TCP phases, like σ-phase, are an area of concern in superalloy metallurgy since they are very brittle, and therefore, they negatively affect superalloy mechanical properties. TCP phases are discussed in a little more detailed in the following paragraphs.

Carbides: Carbon that is added to GTD111 alloy at levels of about 0.08-0.12%, combines with reactive and refractory elements (Ti, Ta, and Hf) and forms MC-type carbides. During production heat treatment and also, during the high temperatures experienced while the engine is in service, these MC carbides tend to decompose and generate lower carbides such as $M_{23}C_6$ and M_6C, which segregate mostly in the alloy grain boundaries. They can be found in several ordered morphologies (plates, regular geometric shapes etc), but in the examined GTD111 samples they were observed in irregular bulky shapes, as depicted in Figure 5.

The main source of carbon in GTD111 below 980°C, as well as in most Ni-based superalloys, is the high-temperature carbide MC. During production heat treatment and high temperature in-service exposure it decomposes slowly, yielding C that permeates the alloy and gives some interesting reactions:

$$MC + \gamma \rightarrow M_{23}C_6 + \gamma'$$

$$MC + \gamma \rightarrow M_6C + \gamma'$$

These reactions yield the lower carbides ($M_{23}C_6$ and M_6C) and γ' phase in various locations but most commonly in the grain boundaries. Both the blocky carbides and the γ' phase produced are important. It is believed that carbides inhibit grain boundary sliding. The generated γ' phase segregates the grain boundaries and envelopes the carbides (see Figure 5) in a relatively ductile, creep-resistant layer.

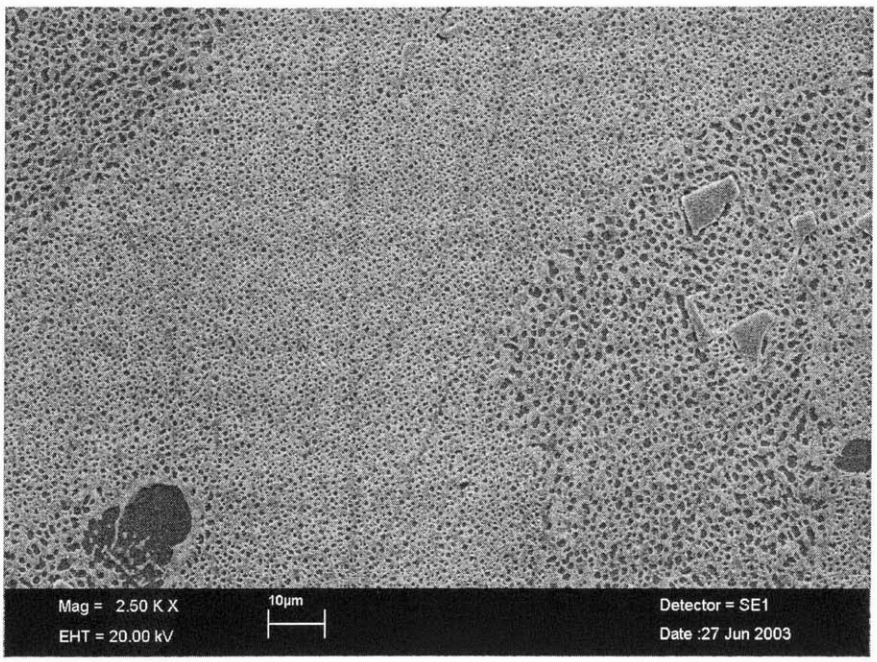

Figure 5 - GTD111 grain boundary morphology

The typically dense, closely packed FCC structure of the grain boundary carbides makes them very strong. Thus, they promote alloy rupture strength by inhibiting grain sliding. However, in some cases it was discovered that material rupture failure was initiated either by fracture of these same grain boundary carbides or by de-cohesion of carbide-to-grain interface.

Overall, the role of carbides in superalloys and their effect on mechanical properties is complex and yet it is not clear whether carbides are to be tolerated or are essential in superalloy grain boundaries [7]. Most investigators believe that carbides have a positive effect on high-temperature rupture strength. Furthermore, it has been verified that carbide morphology influences alloy ductility and that, due to carbide transformation throughout service life, they have a clear effect on the chemical composition stability of the γ-matrix (they remove reacting elements).

TCP Phases: Under certain conditions – e.g. composition not carefully controlled and selection of improper initial heat treatments among others – undesirable phases can form either during solution heat treatment or, more commonly, during service. These precipitates, called Topologically Close Packed (TCP) phases, are composed of close-packed layers of

atoms forming in "basket weave" nets. In several Ni-based alloys, TCP phases (i.e. σ, μ, η, and Laves phases) occur in plate-like morphology, which in 2-D microscope appears as needles.

Often, nucleation of σ-phase occurs on or near carbide particles, at grain boundaries. There, the concentration of elements critical to σ-phase formation (Cr & Mo) is usually high. It is quite interesting that σ-phase is structurally related closely to the common $M_{23}C_6$ carbide. If all C atoms were removed from an $M_{23}C_6$ carbide lattice, only a slight shift in atom-to-atom dimensions would yield the σ structure. Considerable lattice coherency exists between σ-phase and $M_{23}C_6$ carbide.

The TCP σ-phase is a hard intermetallic compound, known to have detrimental effects on the mechanical properties of the alloy; it lowers the high-temperature rupture strength and it can lead to low-temperature brittle fracture [7]. These effects are basically attributed to the following reasons:

a. The σ-phase plates are brittle and by being nucleated at the grain boundary carbides, they offer an ideal path for initiation and propagation of cracking.
b. The σ-phase contains a large quantity of refractory elements (Cr, Mo, and W) that are depleted from the γ-matrix structure. Thus, the solution strengthening effects in the γ matrix diminish.

In the GTD111 samples the σ-phase was found to be in extremely low volume fraction (located sparsely within the alloy microstructure) and only in the after-service material. However, it is known [8] that TCP phases are not a concern for GTD111 alloy degradation.

Grain Boundary Microstructure: In GTD111 alloy, as well as in several other strong Ni-based superalloys, heat treatments and service high-temperature exposures generate a network-forming film of eutectic γ′ phase along the grain boundaries (Figure 5). As discussed before, the degeneration of MC carbides leads to grain boundaries abundant with $\gamma'/M_{23}C_6/M_6C$ layers. The concentration of γ′ at grain boundaries in GTD111 (and other Ni-based superalloys) provides a significantly better combination of strength and ductility than the single-carbide microstructure. By enclosing the typically hard carbides in an environment that allows "controlled" slip, the onset of intergranular fracture is inhibited. Thus, the rupture life of the material is promoted. However, excessive development of these layers can have

negative effects on the mechanical properties; when the $\gamma'/M_{23}C_6/M_6C$ films become too thick, the boundary is embrittled and becomes notch sensitive and prone to cracking. Continued growth of the γ' phase eventually reduces the creep resistance of the material [7].

Hafnium (Hf) addition to Ni-based alloys has an $M_{23}C_6/M_6C$ carbides quantity controlling action; it is extremely active carbide former (it primarily forms stable HfC), and thus, excessive $M_{23}C_6/M_6C$ formation is inhibited. In addition, it solution-strengthens the γ' particles. In overall Hf, which previous researches [6] have estimated to be concentrated in GTD111 in 0.02-0.08 %, promotes alloy mechanical properties by allowing for plastic strain accommodation without effecting high creep resistance [7].

4. Previous Work on GTD111 Alloy Rejuvenation

After some literature research for previous work performed on GTD111 material rejuvenation, it was found that several studies were done between 1994 and 1999 [4, 8, 9]. The results and conclusions from previous researchers that are related to the present thesis could be summarized as follows:

4.1 Material Degradation

When exposed to high-temperature/high-stress environment (as in the case of turbine engine applications) the GTD111 alloy degrades. The degradation involves the material microstructure and the mechanical properties as a result of microstructural morphology changes.

As far as the microstructure is concerned, the primary γ' precipitates tend to coarsen, coalesce, and take a more spheroid rather than cuboidal shape. It was also observed [9] that a significant fraction of secondary γ' particles dissolved. A continuous γ' phase network is formed along the grain boundaries, while some grain boundary carbides precipitated during service were also noticed [9].

The mechanical properties of the alloy, and particularly the creep rupture characteristics, which are one of the most significant properties for turbine superalloys, are highly influenced by the microstructural features. As a result of the service-induced microstructural changes, the creep rupture resistance is diminished. It has been found that after-service GTD111 exhibited three or more times lower rupture life than the original material [8]. Additionally, hardness and tensile properties also degrade during service due to microstructural degradation [9]. Finally, it has been reported that impact strength of several superalloys exposed to high temperatures is significantly reduced with aging/service time [10].

4.2 Microstructure Restoration

Based on the published data, the tested GTD111 rejuvenation heat treatments can be categorized as follows:

a. "Standard" heat treatment that is designed for the optimization of the virgin material [8], and consists of partial solution treatment (2050°F for 2 hours) followed by aging heat treatment (1550°F for 24 hours) [8, 9].

b. "High temperature" heat treatment that consists of the "standard" heat treatment with the addition of a high-temperature solution treatment for 2 hours that is performed prior to the "standard" heat treatment. The exact level of "high temperature" varied between different researchers between 2150°F [4] and 2175°F [8].

The standard heat treatment has not been quite effective in restoring after-service alloy microstructure features to the original condition [8]. The primary and secondary γ' particles remained rounded and significantly coarser after the standard heat treatment than in the original material. On the contrary, the "high temperature" heat treatments produced cuboidal primary and fine spherical secondary γ' particles.

4.3 Mechanical Properties Restoration

As expected, based on the properties-to-microstructure relation, high temperature heat treatments succeeded in restoring the material mechanical properties ([4, 8]). Solution treatment at 2150°F/2hr followed by the "standard" heat treatment (2050°F/2hr and 1550°F/24hr) gave the material the up-to-then (1994 timeframe) known best stress rupture properties [4]. Additionally, the 2175°F/2hr high temperature treatment not only improved tensile and yield strengths, but also increased the after-service material creep rupture life by a factor of four, bringing it back to the original material levels [8].

5. Metallographic Analysis Results

For each one of the GTD111 alloy conditions examined (paragraph 2.2 above, categories a. through f.) the analysis results are as follows:

5.1 Original Material

No porosity was observed in the examined samples and this is an indication that the parts were hot isostatically pressed during manufacturing [6]. The γ' phase volume fraction was calculated to be approximately 24%. In the dendrites area of original (un-degraded) material the γ' precipitates were observed evenly distributed in the FCC γ-matrix in two different shapes:

a. Primary γ' precipitates with mostly cubical shape that presented varying degrees of spheroidization (Figure 6). The edges and corners of the average shape were slightly curved, whereas an appreciable percentage of the particles was found to have a purely cubic or prizmatic shape (Figure 7).
b. Secondary γ' precipitates with spherical shape and average size of 0.1 μm. The secondary γ' particles were spread among the primary γ' particles in the grain region.

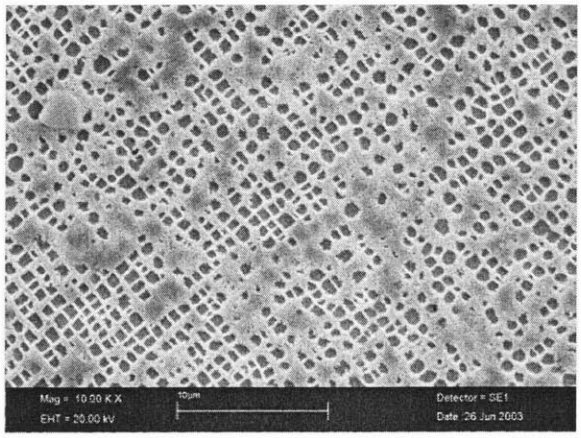

Figure 6 - Original material primary γ' precipitates

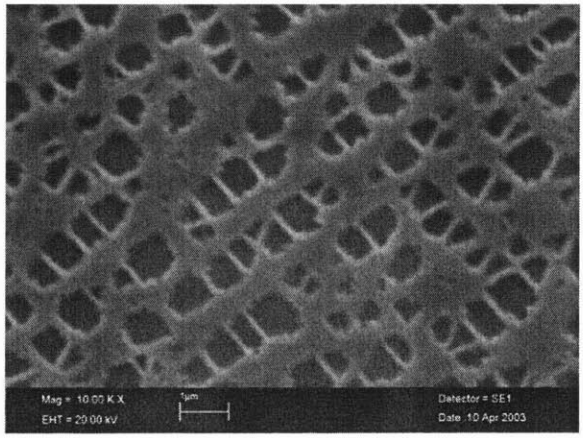

Figure 7 - Original material cubic and tetrahedral γ' precipitates

More micrographs can be found in Appendix B.

A total of 9607 particles were measured; the measurements of primary γ' precipitates dimensions the in the original GTD111 alloy condition, are summarized in Table 2, whereas more detailed statistics of the measurements can be found in Appendix C. It should be noted that the measurements are also presented separately for the two buckets examined (S/N 083 & 849) since they had undergone different service exposure aging. The γ' particle coarsening calculations that follow (paragraph 7.2 below) necessitated the individual examination of each one of the buckets so that sound conclusions could be derived.

	Measurement	**Category Average**	**S/N 083** (3892 particles)	**S/N 849** (5715 particles)
a.	Particle Area (μm^2)	0.262	0.310	0.229
b.	Particle Major Dim. (μm)	0.649	0.709	0.608
c.	Particle Minor Dim. (μm)	0.461	0.500	0.434
d.	Equival. Sphere[2] Radius (μm)	0.298	0.325	0.280

Table 2 – Original material measurements summary (mean values)

The inter-dendritic region was dominated by coarse, irregular round shaped γ' particles, which occupied rather extensive zones between the grains. Large γ' eutectic nodules were also observed occasionally in the grain boundaries, and carbides, usually enveloped by γ' phase particles, were noticed in both the grain interiors and grain boundaries.

[2] As defined in paragraph 2.4 above

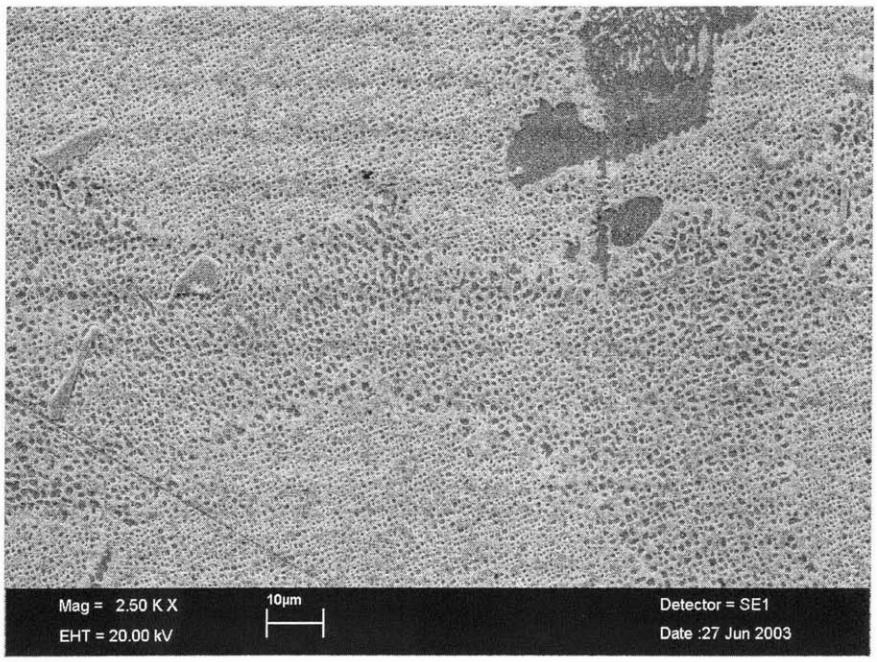

Figure 8 - Original material grain boundary microstructure

The root region of the buckets operate at relatively low temperatures compared to the airfoil region and thus are not expected to degrade during service. Therefore, the microstructure observed at the root section corresponded to material original condition and these measurements were used to quantify the microstructural degradation in the airfoil after service exposure as well as the attempted rejuvenation of the microstructure after given heat treatments.

5.2 After-Service Material

The material examined in the after-service condition exhibited a relatively stable microstructural configuration. Although some differences were identified and are discussed in the following paragraphs, the overall image of the microstructure had significant resemblance to the original material micrographs. The two buckets examined had different service history; nevertheless, the alloy from the two buckets had similar microstructural features, with limited differences, as noted below. No porosity was identified, which is an additional indication of proper HIP process applied during manufacturing.

The γ' phase volume fraction averages approximately 28.5% for the samples from both buckets; in particular it was calculated to be approximately 29% for bucket S/N 083 and 28.1% for S/N 849. The relative increase in γ' phase volume fraction from the original material (24%) is in agreement with the γ' precipitate coarsening observation, as detailed in the following paragraphs.

The γ' precipitates do not exhibit significant differences with the original material; once more, they presented a bimodal configuration. Primary γ' particles are spread evenly in the γ-phase matrix, and they have a basically cuboidal shape with varying degrees of roundness (Figure 9). Both nearly cubic and nearly spherical shapes were observed in the same sample, as can be noticed in micrographs included in Appendix B. Secondary γ' particles still exist, which, based on previous reports [6], is an indication of a rather limited material service-induced degradation. In addition, no profound spherodization of primary γ' particles was noticed, especially in the bucket S/N 849 samples.

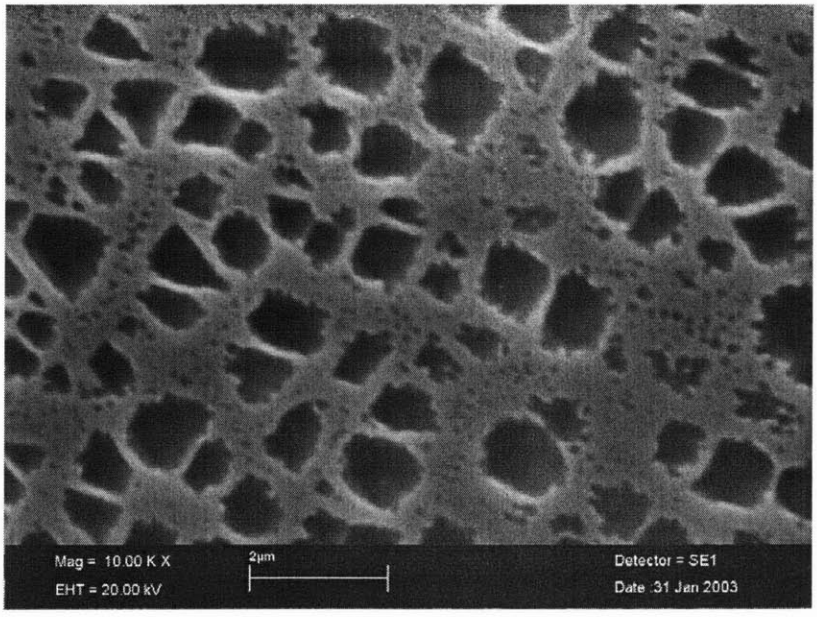

Figure 9 - After service material typical γ' precipitates configuration

A total number of 5828 particles were analyzed; 3270 from bucket S/N 083 and 2558 from S/N 849 samples. The measurements of primary γ' particles dimensions are

summarized in Table 3 below and additional statistics are provided in Appendix C. It is worth noting that the measurements from both buckets indicated a limited-to-moderate increase in the γ' precipitate size as a result of high-temperature service exposure, which is in accordance with the conclusions of previous researchers [6, 8, 9].

	Measurement	Category Average	S/N 083	S/N 849
a.	Particle Area (μm^2)	0.323	0.362	0.273
b.	Particle Major Dim. (μm)	0.726	0.770	0.669
c.	Particle Minor Dim. (μm)	0.499	0.522	0.470
d.	Equivalent Sphere Radius (μm)	0.328	0.345	0.306

Table 3 - After service material measurements summary (mean values)

The grain boundary regions of after-service material appear to have the same morphology as the original material; coarse, irregularly shaped γ' particles prevail and form a γ' "net" along the boundaries. In several locations the γ' net envelopes degenerative carbides that result from MC carbides reaction (Figure 10), while it is often "interrupted" by γ' eutectic nodules (Figure 11). In very few instances TCP phase (plate shaped σ-phase) was identified within γ' eutectic nodules (Figure 11); the extent, though, of σ-phase was too small to characterize in a quantitative manner.

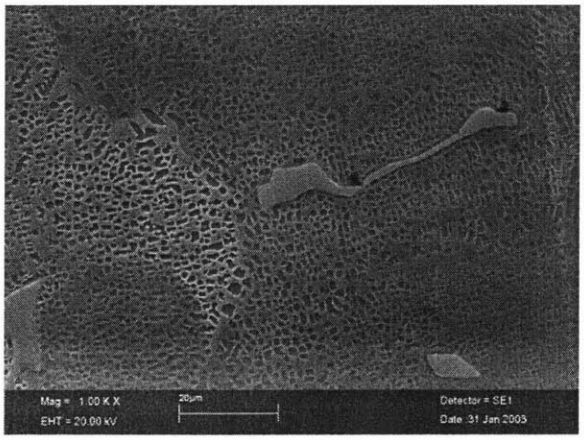

Figure 10 - Grain boundary carbides in after-service material

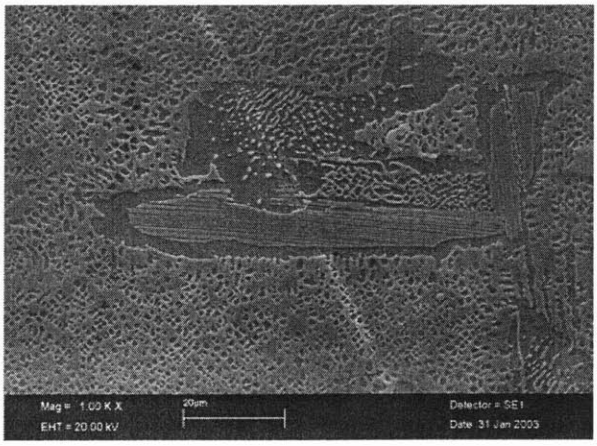

Figure 11 – Gamma prime nodule/σ-phase in after-service material grain boundary

Although buckets S/N 083 and 849 had approximately equal time of service (38000 and 36000 hours respectively), and the overall microstructural morphology is very similar, there were two differences noted in the microscopic examination:

a. Primary γ' precipitates in S/N 083 samples show a tendency for neighboring particles coalescence (Figure 12) with a resulting increase in particle size. This observation is in agreement with the larger γ' particle size measured in S/N 083 samples.
b. Primary γ' precipitates in S/N 849 samples appear more resistant in loosing the cubical shape and becoming rounded, than in the bucket S/N 083. As depicted in Figure 13 the S/N 849 γ' particles have a much more cubic shape, almost identical to the shape observed in the original material samples.

Both differences mentioned in the previous paragraph indicate that although both buckets had similar operational history and they were in rather good microstructural condition, S/N 083 was slightly more degraded.

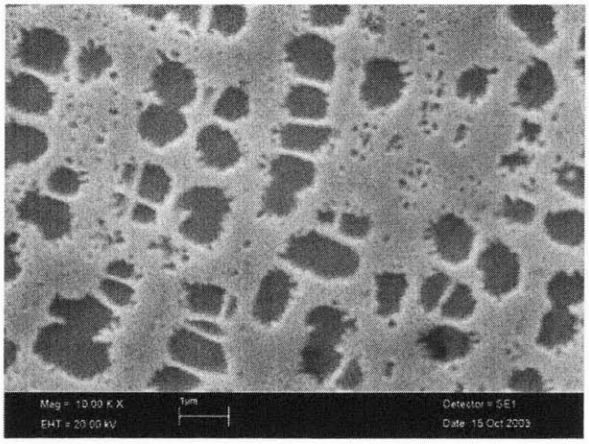

Figure 12 - Bucket 083 γ' particles after service

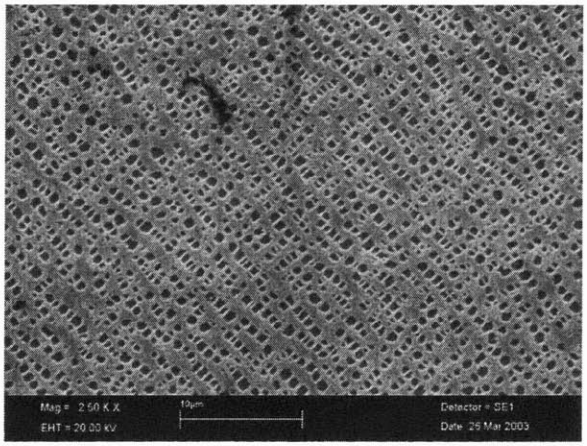

Figure 13 - Bucket 849 γ' particles after service

5.3 Aged Material

Examination of samples after aging heat treatment (1550° F / 24 hrs) performed on after-service material revealed no particular change of the microstructure features. The primary γ' precipitates have a cuboidal shape ranging from purely cubic to purely spherical (Figure 14). Secondary particles are still present among the primary γ' precipitates. In samples from bucket S/N 083 it was also noticed that adjacent particles

tended to agglomerate and form larger particles, as it was observed in the S/N 083 after-service samples (Figure 15). Additional micrographs can be found in Appendix B.

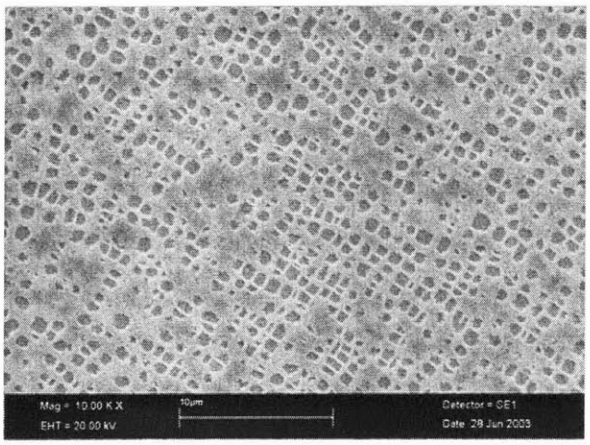

Figure 14 - Aged material γ' particles morphology

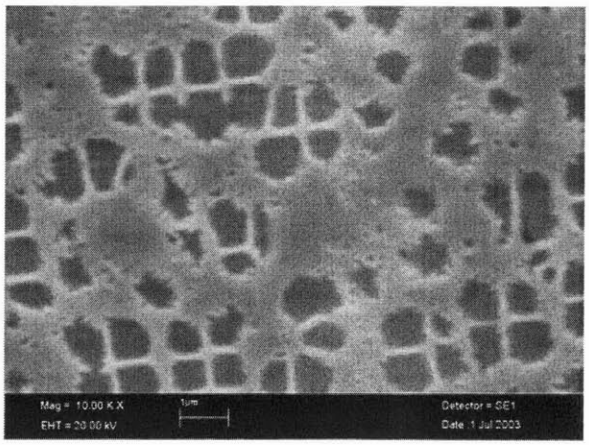

Figure 15 - Aged 083 γ' particles coalescence

A total number of 9640 particles were analysed; 5705 from bucket S/N 083 and 3935 from S/N 849 samples. Primary γ' particles dimensional measurements are summarized in Table 4 below and detailed statistics are included in Appendix C. After comparison with the after-service condition measurements, the aged material shows very limited coarsening of γ' particles. In particular the particles in S/N 083 bucket samples showed a size[3] increase of 10.7%, which can be attributed to neighbouring particle coalescence. On the other hand, measurements in S/N 849 bucket samples presented a decrease in γ' particles size by 2.9 %. Practically, after taking into account the statistical variability of the measurements, it can be concluded that aged material γ' particles have approximately the same size as in the pre-aging-heat-treatment condition (after-service material).

	Measurement	Category Average	S/N 083	S/N 849
a.	Particle Area (μm^2)	0.359	0.429	0.259
b.	Particle Major Dim. (μm)	0.775	0.855	0.660
c.	Particle Minor Dim. (μm)	0.525	0.575	0.454
d.	Equivalent Sphere Radius (μm)	0.347	0.382	0.297

Table 4 - Aged material measurements summary (mean values)

[3] Based on the equivalent sphere approach detailed in paragraph 2.4 above.

As far as the grain boundary microstructure is concerned, aged material observations did not show any noteworthy difference as compared to the previous material condition categories: large γ' particles formed a net across the boundaries, where carbides and bulky γ' nodules were also noted (Figure 41 through Figure 43 in Appendix B).

Based on the observations and measurements on aged material samples, it is believed that the aging heat treatment at 1550°F for 24 hrs did not have any substantial effect on the already degraded microstructure; possibly a very limited coarsening of primary γ' particles, but certainly not any type of restoration of after-service material to the original condition.

5.4 HIPed Material

After HIP treatment (15 Ksi at 2200° F for 4 hours) of after-service GTD111 material, the morphology of the microstructure has changed drastically. The γ' particles have irregular shapes, close to "crushed" cuboidals whose sides have been distorted as a result of the high pressure applied (Figure 16, Figure 44, and Figure 45 in Appendix B).

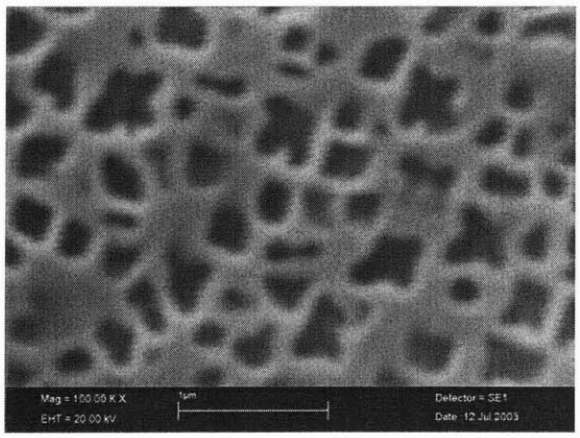

Figure 16 - Gamma prime particles after HIPing

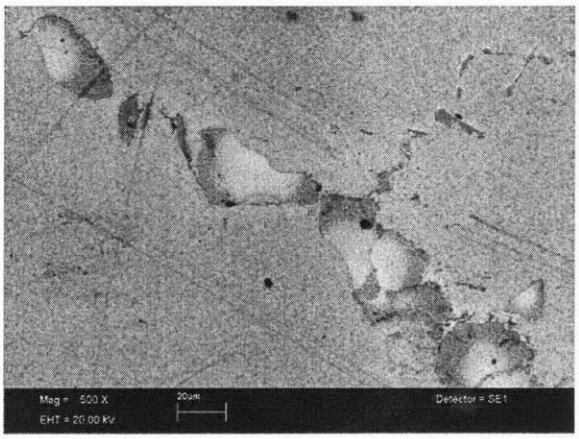

Figure 17 - Grain boundaries at HIPed material

The effect of HIP treatment on the γ' particles size can be calculated from the dimensional measurements taken, which are summarized in Table 5. Again, more measurement statistics can be found in Appendix C. A total of 324 γ' particles from both

buckets were examined, and the γ' volume fraction was measured approximately 29.6%. Due to the very small size of the particles it was necessary to use as high magnification as 100,000X in order to efficiently perform the required measurements.

	Measurement	Category Average
a.	Particle Area (μm^2)	0.046
b.	Particle Major Dim. (μm)	0.286
c.	Particle Minor Dim. (μm)	0.191
d.	Equivalent Sphere Radius (μm)	0.127

Table 5 - HIPed material measurements summary (mean values)

Radical changes were also observed in the grain boundary regions; the coarse γ' particles net had been replaced by large γ-γ' nodules formed along the boundaries (Figure 17 and Figure 46, Figure 47 in Appendix B). Much less and smaller carbides were observed in the grain boundaries region, and this observation is in agreement with previous researchers observations suggesting that carbides usually dissolve during HIP treatment [9].

Based on the shape of primary γ' precipitates ("crushed" cuboidals) it is believed that the HIP treatment did not resolve and re-precipitate γ' phase in the alloy; its effect on the γ' particles morphology was rather limited to the mechanical deformation of existing precipitates.

5.5 HIPed/Aged Material

The samples of this material condition showed almost identical microstructural characteristics with the HIPed-only condition material. The shape of γ' particles in the γ-γ' matrix is the same as in the previous category: cuboidals with sides that yielded under the high pressure, as indicated in Figure 18. The morphology of grain boundary microstructure does not present any difference after the aging treatment (1550° F /24 hrs), and it is also characterized by large γ-γ' eutectic nodules (Figure 19).

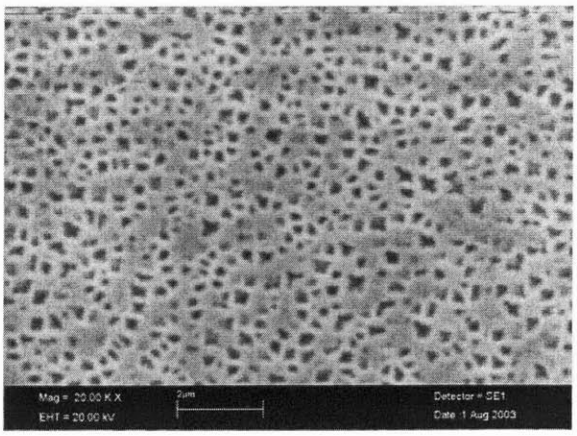

Figure 18 - Gamma prime particles after HIP and aging

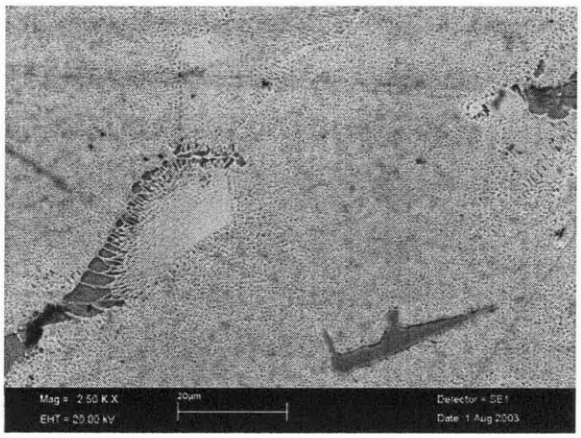

Figure 19 - Grain boundaries after HIP and aging heat treatments

Table 6 summarizes the γ' particles measurements taken from the four HIP-aged condition samples (3514 particles analysed) and more statistics can be seen in Appendix C. It can be easily noticed that aging did not have any noticeable effect on the γ' particles size.

	Measurement	Category Average
a.	Particle Area (μm^2)	0.040
b.	Particle Major Dim. (μm)	0.256
c.	Particle Minor Dim. (μm)	0.183
d.	Equivalent Sphere Radius (μm)	0.118

Table 6 - HIP-aged material measurements summary (mean values)

5.6 HIPed/Solution/Aged Material

As noted in a previous paragraph, a number of HIPed samples underwent a solution heat treatment (2150°F/2hrs and 2050°F/2hrs) that was followed by aging heat treatment (1550°F/24hrs). Analysis of samples in this condition revealed a dramatically different microstructural morphology, compared to the one noted in the HIPed only and HIP/aged samples. The γ' precipitates regained a regular shape which in most

micrographs was purely cubic (Figure 20). No secondary γ' particles were observed, as was also noted in previous works [4].

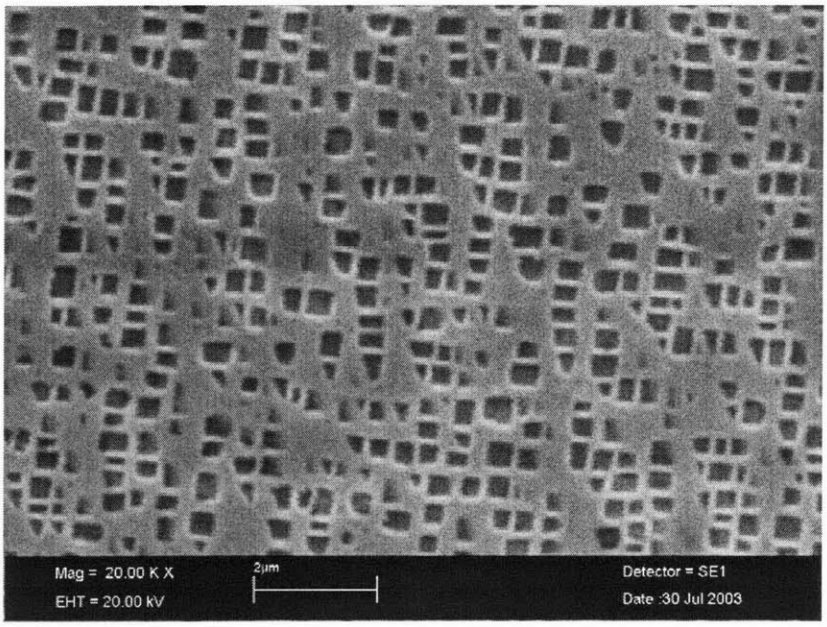

Figure 20 – HIP/solution/aged material γ' particles

The size of primary γ' particles is significantly larger than in the other two HIPed material conditions. Out of 3802 particles analyzed, the measurements averages are listed in Table 7; it should be noted that the "equivalent sphere radius" (the particles size metric used throughout the project), was increased by approximately one third, compared to the respective measurement of HIPed and HIP/aged categories. The measured γ' phase volume fraction (23.5%) is very close to the volume fraction measured for the original condition material (24%).

	Measurement	Category Average
a.	Particle Area (μm^2)	0.079
b.	Particle Major Dim. (μm)	0.350
c.	Particle Minor Dim. (μm)	0.266
d.	Equivalent Sphere Radius (μm)	0.167

Table 7 - HIP-solution-aged material measurements summary (mean values)

The grain boundary microstructure presented similar morphology (Figure 21) with the original material; segregation of larger, irregularly curved γ' precipitates, which formed a net in the grain boundaries. In several cases carbides were observed to be enveloped by the bulky γ' particles, as well as γ' eutectic nodules sited in the grain boundaries. However, the γ' eutectic nodules were significantly smaller and fewer than the ones experienced in the HIPed and HIP/aged conditions.

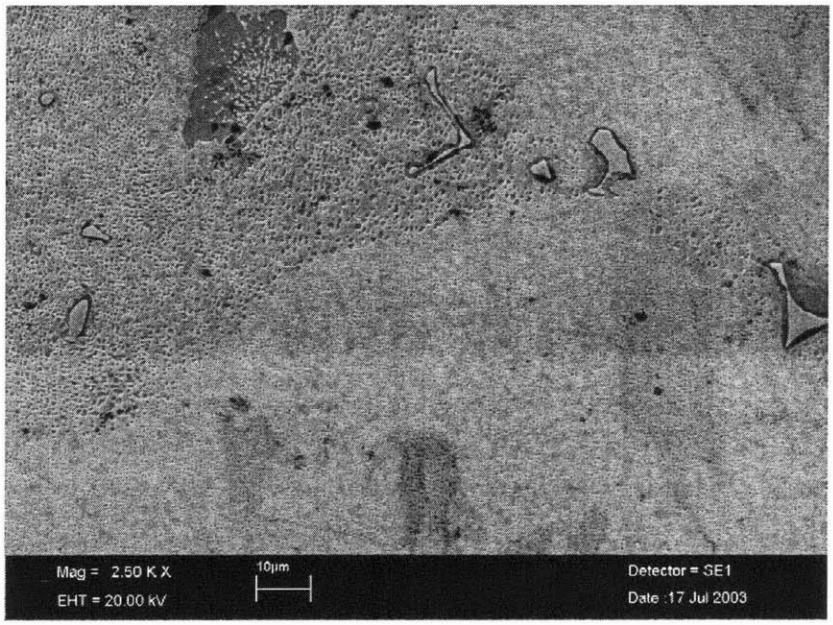

Figure 21 - HIP/solution/aged material grain boundary morphology

From the microstructural morphology observed, it could be concluded that the two high temperature heat treatments applied after the HIP process (2150°F/2hrs and 2050°F/2hrs), resulted in solution and new precipitation of γ' phase within the alloy. This is in agreement with the mechanical properties improvement that was observed in GTD111 material after similar heat treatments sequence in service-degraded samples [4, 8].

6. Metallographic Analysis Summary

The results and observations of the metallographic analysis can be summarized as follows:

6.1 Gamma Prime Precipitates Size

The average γ' precipitates size measurements for all examined alloy conditions are depicted in Figure 22. Based on the measurements, the following points can be made:

a. Original condition GTD111 alloy from both buckets examined (S/Ns 083 & 849) had similar microstructure morphology but different γ' precipitate sizes; particles in S/N 083 were 16% larger.
b. The size of γ' particles was clearly affected by high temperature service exposure for both buckets. After 36000 or more hours in service, the size of γ' precipitates (equivalent sphere radius) was increased by approximately 10%.
c. Aging heat treatment of after service material (1550°F/24hrs) appeared to have some influence on S/N 083 bucket γ' particles size. However, in that particular bucket sample it was noticed that a lot of neighbouring particles tended to coalesce, leading to the observed increase in the average size. Individual particle size increases were very limited, as indicated also by bucket S/N 849 results, where no particles coalescence was noticed and particles size was measured almost unchanged.
d. HIP treatment (15Ksi/2200°F/4hrs) drastically decreased γ' particles size. Based on the microscopic observations, though, the measured size decrease can be solely attributed to particles volume mechanical deformation. No new precipitation of γ' phase was observed.
e. Aging treatment (1550°F/24hrs) applied after HIP did not change γ' precipitate sizes.
f. Combined solution/aging heat treatment (2150°F/2hrs - 2050°F/2hrs - 1550°F/24hrs) resulted in solution and new precipitation of γ' phase particles

with approximately half the size of γ' precipitates in the original GTD111 material.

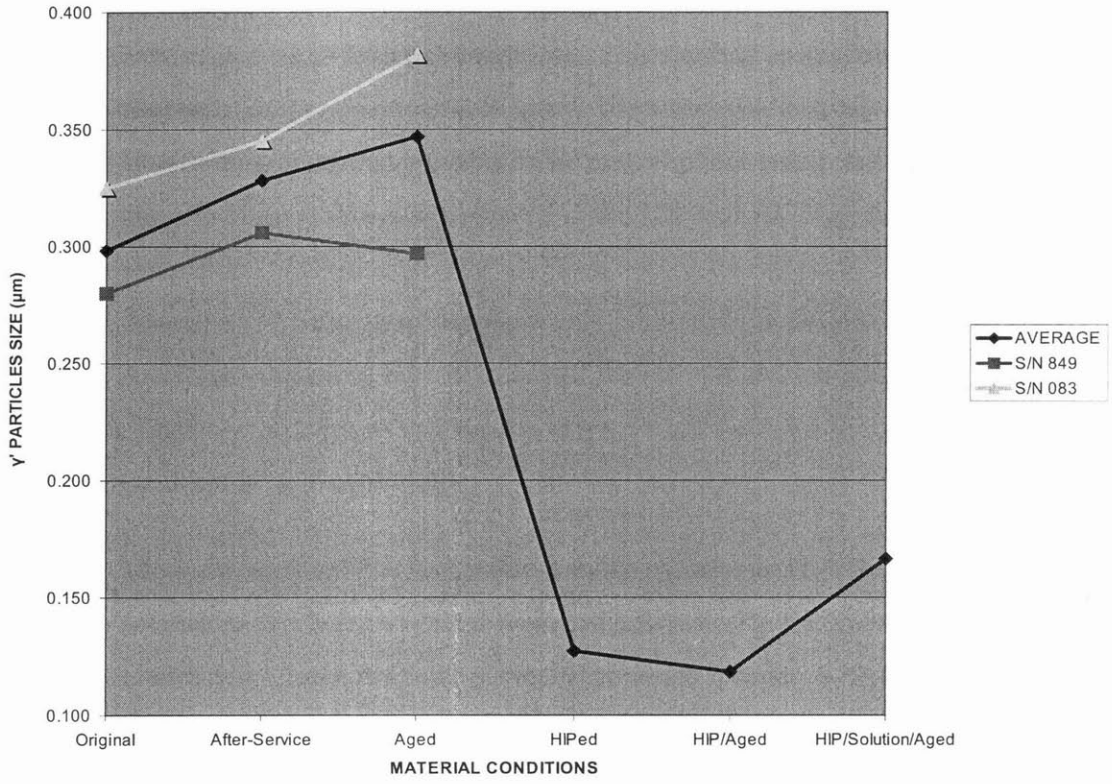

Figure 22 - Evolution of γ' particle size w/ categories

6.2 Gamma Prime Precipitates Shape

As noted in a previous paragraph, within GTD111 alloy grains the γ' phase appears in two different shapes: large primary cuboidal particles and small secondary spherical precipitates. The observations from the performed analysis can be summarized as follows:

a. Primary γ' particles had cuboidal shape with varying degrees of roundness in the Original, After-service, Aged and HIP/Solution/Aged conditions. Particularly in the later, more purely cubic particles were observed than in the rest of the categories.

b. No profound rounded particles were noted in any of the categories. Although various degrees of spherodization were observed, in no case there was a massive transformation of γ' particles to fully curved shape observed.
c. Coalescence of neighbouring particles was noticed in bucket S/N 083 After-service and Aged material conditions. This resulted in irregular γ' particle shapes.
d. Due to high-pressure applied with no new γ' phase precipitation, "crushed-cubic" volume shape was observed in the HIP and HIP/Aged condition samples.
e. Secondary γ' phase particles were only present in the Original, After-service, and Aged conditions but not in any of the HIP-related material conditions.

6.3 Grain Boundary Morphology

a. The samples from Original, After-Service, Aged, and HIP/Solution/Aged conditions presented a typical Ni-based superalloy grain boundary morphology: large irregular curved γ' particles forming a "net" across the boundary, with carbides enveloped in several cases. Frequently, γ' eutectic nodules were present in the intergranular region.
b. In very few cases, TCP phase plates (σ-phase) were observed within γ' nodules of After-Service and Aged conditions.
c. The grain boundary region of HIP and HIP/Aged conditions samples were characterized by extremely large γ-γ' eutectic nodules around each grain.

7. Project Results vs. Theoretical Correlations

7.1 Gamma Prime Coarsening Theory

It has been documented [11] that coarsening of γ' precipitates (also called "ripening") takes place in the Ni-based superalloys microstructure, under the driving force of interfacial energy minimization in the γ-γ' interface stress field. As a result and due to chemical potential gradient associated with curved interfaces, large precipitates tend to grow and small to dissolve. This also true for γ-γ' matrix characterizing all superalloys including GTD111; however, due to the cuboidal rather than spherical shape where curvature radius could not be clearly defined, γ' particles coarsening is more difficult to analyse.

In addition to the difficulty presented in the characterization of γ' particles coarsening in superalloys due to their shape, material samples from in-service components – as was the case with the samples used in the project – present some addition concerns. In-service parts and particularly turbine blades are not loaded uniformly since time-related temperature and stress gradients are applied. For that reason, some regions of a particular part have been found to have much more coarse γ' particles than others, also from the same part. In addition, it has been found [11] that coarsening is significantly higher in the upper parts of the blades. It is worth mentioning that all samples examined in the present project were cut from <50% span locations of in-service GE Frame 7 turbine buckets. On the other hand, it has been documented [12] that γ' particle coarsening in superalloy systems is not dependent on the γ' phase volume fraction.

Gamma prime particle coarsening in superalloys has been reported to happen in two distinct stages: first stage where particles growth obeys "cube root time law", and is analyzed in more details in the following paragraphs, and second stage where coarsening rate is much slower, and results in platelet-shaped particles ("rafting"). No rafting of γ' precipitates was observed at any of the GTD111 conditions examined.

The rate of γ' particles coarsening in superalloys including GTD111 has been documented [6] to follow diffusion-controlled coarsening kinetics. As described by

Chellman and Ardell [13], the Lifshitz, Slyozov, and Wagner theory (the "LSW" model) holds, and it can be expressed by the "cube root time" equation:

$$(r_F^3 - r_S^3)^{1/3} = K \cdot t^{1/3} \tag{2}$$

where t is time in seconds, r_F is the average γ' particle radius in nanometers at time t, r_S is the average γ' particle radius at t=0. K is a constant [14] :

$$K = \left(\frac{8}{9} \cdot \frac{D \cdot \gamma \cdot V_m \cdot C_e}{R \cdot T} \right)^{1/3} \tag{3}$$

where D is the composite diffusion coefficient for the various elements, γ the free energy of the γ'-particle/γ-matrix interface, V_m the molar volume of the precipitate, C_e the concentration of γ'-forming elements in equilibrium with a precipitate of infinite radius, R the gas constant and T the absolute temperature.

The temperature-dependent terms in equation (3) are D and C_e. The diffusion coefficient D has a dependence of the form $D=D_0e^{-Q/RT}$ where Q is the activation energy for the diffusion of the γ'-forming elements (primarily Al and Ti) within the γ-matrix. By assuming equilibrium volume fraction of γ'-phase constant and concentration C_e also constant, Stevens and Flewitt [14] concluded that the relation defining K can be written:

$$\ln(K^3 \cdot T) = B - \frac{Q}{R \cdot T} \tag{4}$$

where B is a constant. A plot of $ln(K^3T)$ versus $1/T$ is a straight line with Q/R being the slope. Thus, for known "start" and "end" γ'-particles sizes (r_S and r_F respectively) and by using equations (2) and (4), once Q is known, metal operating temperature (T) can be estimated.

The activation energy for diffusion has been reported in the literature for both simple systems as Al in Ni and Ti in Ni as well as complex superalloys such as IN-738, U500 etc. The reported value of Q varied from 2.57 to 2.83x10^5 Joules/mole. Specifically for GTD111 diffusion activation energy has been calculated by Daleo and Wilson [6] to be 2.59x10^5 Joules/mole.

In the same study [6] a carefully controlled heat treatment was performed where material with initial γ'-particle size r_S =0.86μm was exposed to T=1650°F for t=5000hrs. The final γ' particle size was measured to be r_F =1.16μm. With the given data, a point in the $ln(K^3T)$ vs $1/T$ diagram can be located. Then by assuming a value of Q=2.6x10^5

J/mole based on previous work mentioned above, the slope of the straight line can be calculated and the whole $ln(K^3T)$ vs $1/T$ plot can be derived for GTD111 (Figure 23).

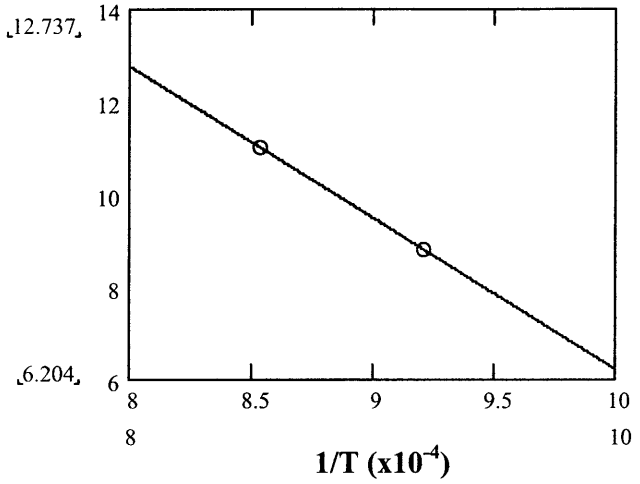

Figure 23 - Plot $ln(K^3T)$ vs. $1/T$ of γ' particles coarsening in GTD111

Thus, in the case of GTD111 alloy, equation (4) expressing the relation of factor K with absolute temperature T can be written as:

$$\ln(K^3 \cdot T) = 38.87 - 3.267 \times 10^4 \cdot \frac{1}{T} \qquad (5)$$

7.2 Project Results vs. Theory Correlation Examination

In the case of the material samples examined in the present study, the known data for the γ'-particles coarsening during service are summarized in Table 8. For γ'-particle sizes the equivalent sphere calculated radius approach was used. Initial size value corresponds to average original condition measurement, whereas for final size the after-service value was used. The value of K-factor was calculated using equation (2).

	Initial size - r_S [nm]	**Final size - r_F [nm]**	**Time – t [sec]**	***K*-factor [nm $sec^{-1/3}$]**
S/N 083	325	345	1.368×10^8	0.3665
S/N 849	280	306	1.296×10^8	0.3725

Table 8 - Coarsening calculations data

Based on the known data, equation (5) was solved for the two buckets operating temperatures resulting in T_{083}=932.2K (659°C) and T_{849}=933.5K (660°C). These temperatures were evaluated against approximated metal operating temperatures in order to draw some conclusions about the correlation of the performed measurements with existing γ'-particles coarsening theory.

In order to better evaluate the calculated operating temperature, some additional information concerning operating conditions should be considered. As stated previously, the material samples were taken from <50% blade-span locations of GE Frame 7FA 2nd stage buckets. No actual metal operating temperature was available for the particular engine location. It was only known that GE Frame 7FA engine, whose hot section involves three vane-blade sets, has firing temperature (1st stage vane inlet) equal to 1316°C and EGT (Exhaust Gas Temperature) equal to 595°C [2]. Air passing through 2nd stage rotating blade has a lower temperature than the firing temperature of 1316°C. In addition, Frame 7FA 1st and 2nd stage buckets are air cooled using a combined film-convection cooling design scheme [15] which significantly lowers metal temperature.

Previous researchers [9] have documented the service metal temperature at the hottest airfoil locations of GE Frame 5 engines 1st stage buckets (also using GTD111 alloy) to be in the range of 760° to 980°C.

It is believed that the nominal metal temperatures for the buckets examined are in the order of 750° to 950°C. Thus, the theoretically calculated service temperature for buckets S/N 083 and 849 (approximately 660°C) appears to be slightly lower, but this can be attributed to the following reasons:

a. The measurements taken refer to parts under stress in service for which the applied stress levels were not available. In addition, these included measurements from both in-stress-plane and perpendicular-to-stress-plane sample categories. It is known, though [11], that stress applied during high-temperature exposure results to rafted particle morphologies. In addition, the stress field affects particle coalescence [12] and therefore, the resulted γ' precipitate size. It is quite interesting that the average major γ'particle dimension was approximately 40-50% larger than the average minor dimension, indicating a possible deviation

from purely cubic shape. It is believed that in that case the "cube root time" law may not completely account for γ'-precipitate coarsening in this alloy.

b. All the analysed samples were from the lower part of the buckets, which has been reported [11] to be generally under-degraded compared to the upper parts. This is in agreement with the service metal temperature being calculated lower than normal.
c. Although there seemed to be a deviation from purely cubic shape as noted above, the shape was assumed to be cubic and the area measured was used to calculate cubic volume. This was set equal to pure spherical volume whose radius was used as the primary γ' particles size metric throughout the project. It is possible that this "translation" was not accurate enough to the level required for the theoretical calculation of the metal operating temperatures.
d. Although the operating time was given as an approximation, the percentage of total operating time spent under constant firing temperature conditions was not specified. Most possibly the average temperature throughout the service time was less than the nominal operating temperature, and therefore, the calculated metal operating temperatures seem fairly reasonable.

To conclude, it is believed that, after taking into account all above-mentioned information, the calculated metal service temperature correlates quite satisfactory with reality. Therefore, it is considered that the γ' particle size measurements performed also follow published particle coarsening theory for superalloys.

7.3 Other Microstructure Transformations

In general, the microstructure characteristics observed in the various material conditions agree with the theoretical description of the alloy, as presented previously in paragraph 3.2 above. However, apart from the γ' precipitate size evolution that has already been dealt with, it is of a particular interest to discuss some other transformations observed in the samples examined, along with their theoretical context. As such, the following issues will be discussed:

a. Gamma prime particle morphologies: It has been documented [11] that during heat treatment of superalloys with the characteristic γ-γ' structure, in addition to the particle size increase, the particles also undergo a change in morphology. The cubic particles tend to group together and coalesce in small numbers (4-10). The next stage of the phenomenon and in particular under applied stress is to have the coalescence increase anisotropically in certain directions and produce a microstructural morphology of platelets. It should be noted that although from stressed parts the platelets morphology was not observed in any of the GTD111 conditions examined. However, the phenomenon of neighbouring particles coalescence was indeed noticed in the after-service and aged samples of S/N 083 bucket, which was the one with the slightly longer service life (Figure 12 and Figure 40 in Appendix B).

b. Solution and re-precipitation of γ'-phase: Previous work [4, 8] has shown that in order to solutionize and re-precipitate the γ' phase in GTD111 superalloy, it is required to apply a high-temperature heat treatment (2150° or 2175°F for 2 hours) prior to a "standard" heat treatment of 2050°F for 2 hours and 1550°F for 24 hours. The combined high-temperature/standard heat treatment sequence has been proved effective in solutionizing γ'-phase and precipitating new γ' particles during cooling. This was also verified in the present study, where the HIP process was followed by the following heat treatments: 2150°F/2hrs – 2050°F/2hrs – 1550°F/24hrs and the resulted microstructure involved precipitation of new cubic γ' particles that were not present after the HIP process. However, since HIP (15Ksi/2200°F/4hrs) had preceded the heat treatment, it is not clear if the new γ' phase precipitation was the result of the high-temperature heat treatment only or of its combination with the HIP process.

In complete conformance with the necessity of high-temperature heat treatment for microstructural rejuvenation, it is worth mentioning that the aging heat treatment applied during the present project (1550°F/24hrs) did not recover the initial γ' particles size/morphology but had only an additional minimal-to-negligible coarsening effect on the already degraded material.

8. Conclusions

8.1 Project Conclusions

In the present thesis project an effort was made to study the γ-γ' structure present in the GE-patented GTD111 superalloy. Material samples were taken from the lower part (less than 50% blade-span) of GE Frame 7FA power engine 2nd stage buckets that had accrued 36000 to 38000 hours operating time. The study included the quantitative analysis of γ' precipitate size in different material conditions including original, after-service, and after selected heat treatments. The scope of the heat treatments was to identify an effective way to rejuvenate service-degraded material and restore the micro-structural features as close as possible to the original condition. Finally, a correlation was performed to the measured γ' particles size in original and after-service conditions in order to determine whether the gathered data agreed with published γ' precipitate coarsening theory; the measurements taken were used with existing coarsening theory and an estimate for the metal service temperature was derived. This estimate was compared to approximated metal operating temperature of the specific turbine engine parts.

The material showed moderate service degradation, as indicated by:

a. Moderate-to-low coarsening of the cuboidal primary γ' precipitates, with no particular spheroidization observed after the service exposure, and no noted consumption of the spherical secondary γ' particles.
b. Neighbouring primary γ' particles coalescence in one bucket's samples.

It is characteristic that the modest microstructural degradation correlates satisfactorily with the rather low service temperature calculated. Material degradation tended to continue when after-service material was subjected to high temperature exposure (1550°F/24hrs aging) even without simultaneous application of mechanical load.

The metal service temperature calculated based on γ' particles coarsening theory is in reasonable agreement with the estimated operating temperature for the particular section of GE Frame 7FA 2nd stage buckets. Therefore, it is concluded that the rate of GTD111 γ'

precipitates coarsening observed in the present project adequately correlates with the existing coarsening theory published data for other basic $Ni_3(Al,Ti)$ superalloys.

High-temperature (2150-2175°F) solution heat treatment is required for dissolving coarse and rounded γ' particles within γ-matrix and subsequent precipitation of new γ'-phase in cubic shapes. Solution heat treatment (2150°F/2hrs and 2050°F/2hrs) applied after HIP process (15Ksi/2200°F/4hrs) and before aging at 1550°F/24hrs restored alloy microstructure close to the original one, although with quite smaller γ' precipitates. Although cooling rate is considered to affect γ' particles size, the cooling rate applied in the project experiments was not known.

8.2 Future Work Recommendations

The research in GTD111 alloy rejuvenation after service exposure should be continued. In the case of the particular engine parts examined in the project it is necessary to analyze upper bucket region samples (from >50% blade-span locations) where the alloy is expected to present much more severe degradation.

No mechanical testing was performed as part of this project. However, in order to draw sound conclusions concerning the after-service alloy condition and identify the most suitable heat treatment for the material rejuvenation, it is required that mechanical testing (creep stress rupture and tensile strength tests) is performed on the different material conditions. In particular the HIP/Solution/Aged material that appeared to have the most similar microstructure to the original alloy from all the different conditions examined, should be also mechanically tested and compared with the original GTD111 properties.

As mentioned previously, high-temperature solution and re-precipitation mechanism is considered as capable for microstructure rejuvenation. In the project experiments, though, high-temperature solution heat treatment was preceded by HIP

treatment; therefore, it was not possible to clearly identify the effects of high-temperature treatment. It is deemed necessary that solution/aging heat treatment will be performed (2150°F/2hrs – 2050°F/2hrs – 1550°F/24hrs) without prior HIPing. The resulting microstructure should then be compared to the original GTD111 alloy condition. As noted before, this study should also include mechanical property testing for completeness of the conclusions.

Possible elimination of HIP treatment would highly favor after-service GTD111 buckets repair economics, since HIP is a high-cost process. It is estimated that HIP process cost is roughly1K$/hr, but other parameters should also be considered, such as dimensions of chamber, number of buckets that can effectively fit in the chamber, and similar factors. GTD111 material examined did not show significant porosity even in the after-service condition and therefore HIP might not be necessary as part of the repair effort.

In the GTD111 research following the present project, the heat treatment cooling rates should be closely controlled and the effects on γ' particles shape/size should be compared for different cooling rates of the same heat treatment. Cooling rate is related to secondary γ' particles precipitation and primary particles coarsening, which both contribute to the exceptional creep rupture resistance property of GTD111 alloy.

Appendix A

MIT/DMSE SEM CALIBRATION INFO

In order to ensure a high level of fidelity in the performed measurements, the SEM at Materials Science & Engineering Department of MIT, is calibrated as follows:

a. After accomplishment of major maintenance activities (repair, parts replacements etc) that involve the microscope imaging system, or
b. Six months after the last calibration.

The calibration involves testing of SEM readings out of known distances on a standard part. The part used for the magnification calibration image distortion check is the *Ted Pella, Inc*[4] part number 615-3 standard [16], which is a 5mm x 5mm single crystal silicon part (Figure 24).

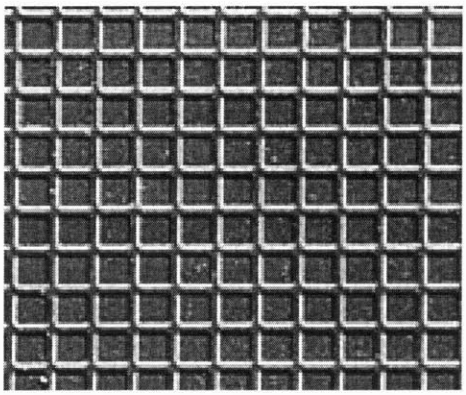

Figure 24 - SEM calibration specimen

The surface of the specimen has a square pattern, where the squares repeat every 10μm (0.01mm). The dividing lines are 1.9μm wide, formed by electron beam lithography. A broader marking line is written every 500μm (0.5mm), which can be used for light microscope calibration testing. All lines and squares are etched, approximately 2μm wide and deep. As noted by the calibration specimen manufacturer [16], it provides a guaranteed dimensional accuracy of 1%, while the basic reference specimen is

[4] http://www.tedpella.com

calibrated by the National Physical Laboratory of England, using laser beam interferometry.

At all tests performed during usage of SEM for the present project, the measurements were within ±2% of the specified distances.

Appendix B

ADDITIONAL MICROGRAPHS

B.1 ORIGINAL

a. Primary γ' precipitates within grains

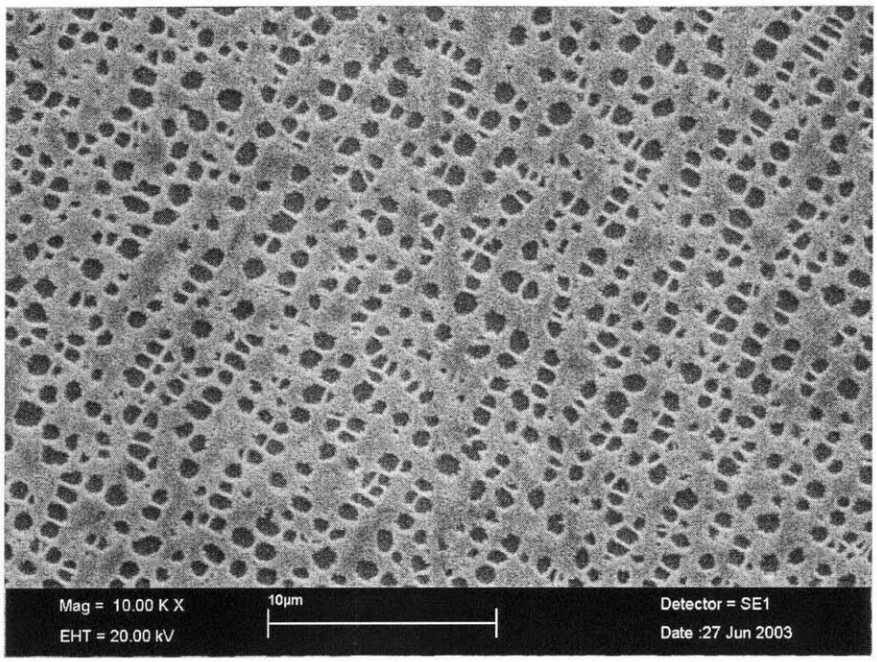

Figure 25 - Original material γ' precipitates

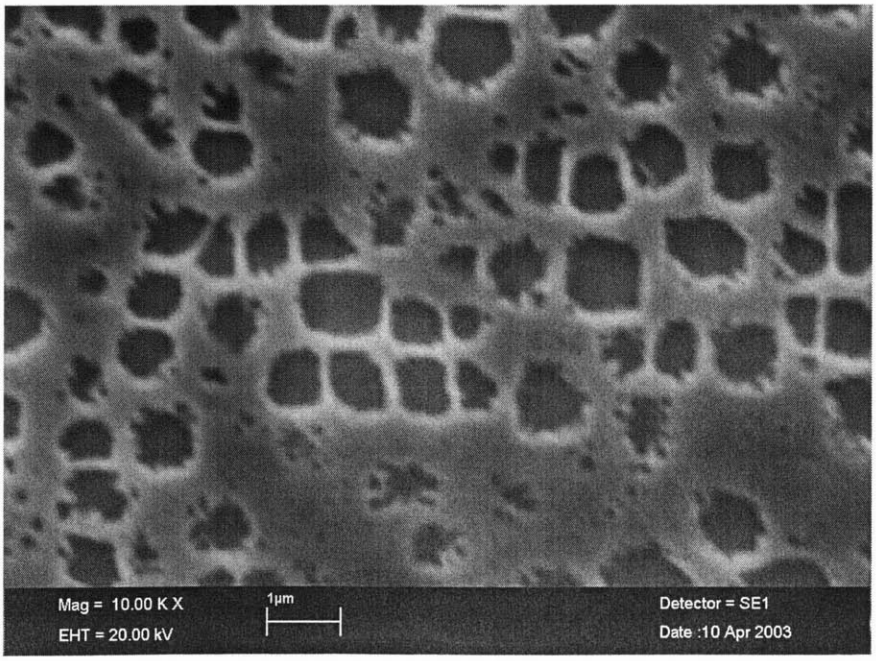

Figure 26 - Original material primary and secondary γ' particles

b. Grain boundaries microstructure morphology

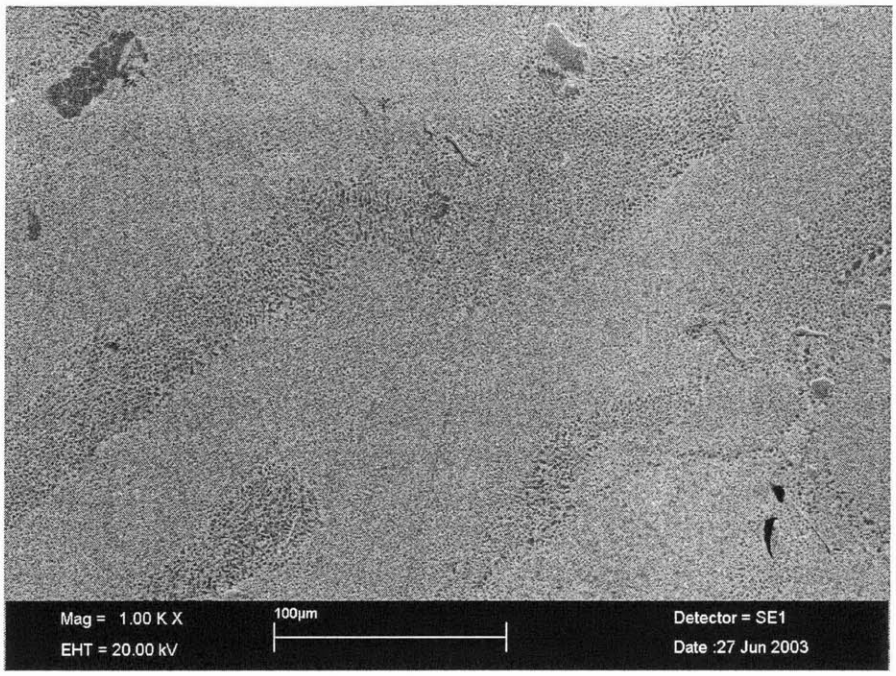

Figure 27 - Original material grain boundary morphology

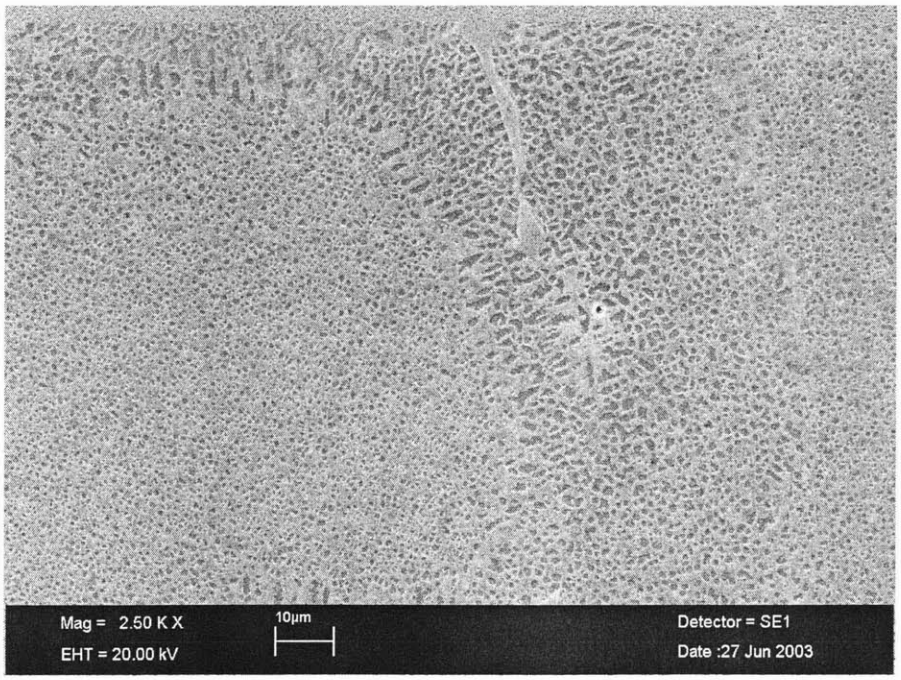

Figure 28 - γ' "film" and carbides along original material grain boundaries

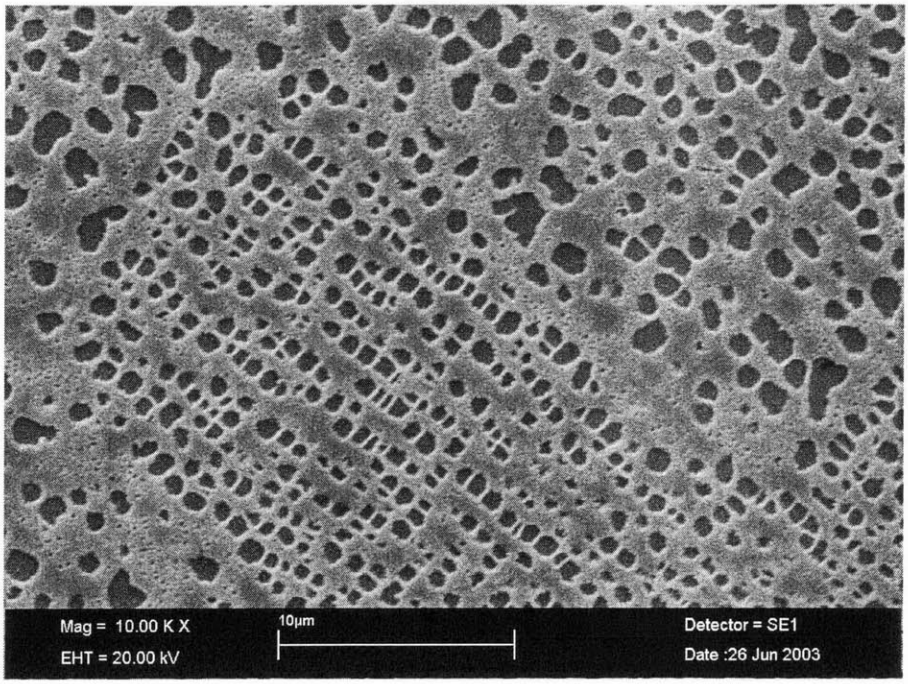

Figure 29 - Primary γ' particles vs. coarse/rounded γ' particles at original material grain boundaries

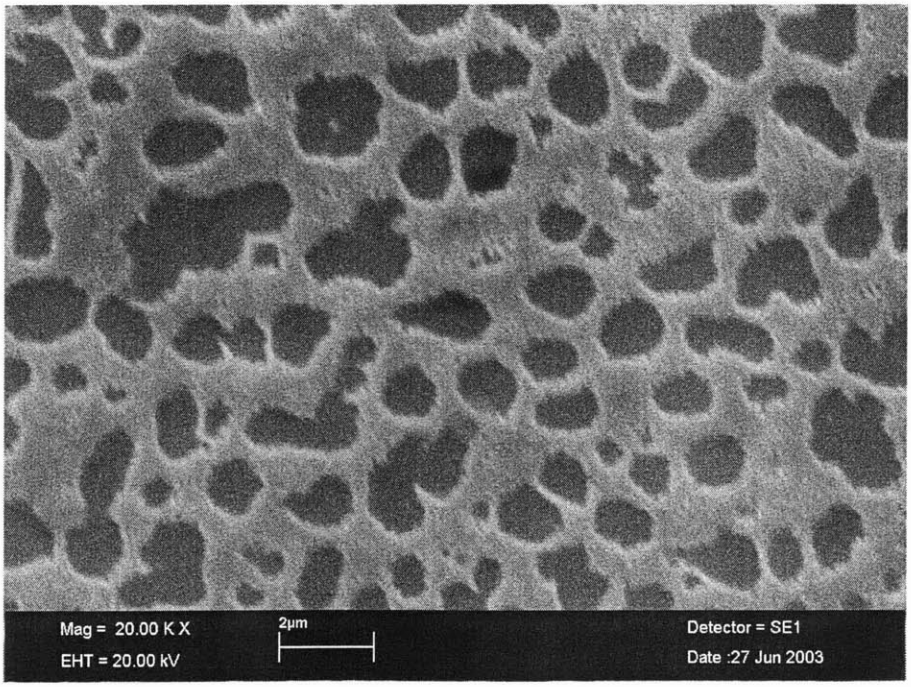

Figure 30 - Original material grain boundary coarse & rounded γ' particles

B.2 AFTER SERVICE

a. Primary γ' precipitates within grains

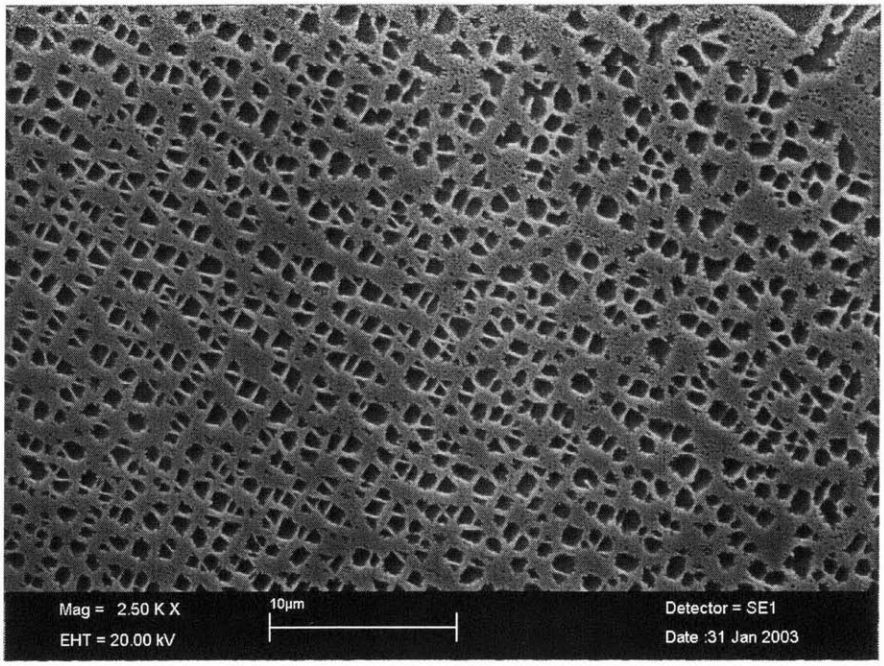

Figure 31 - After-service material γ' particles

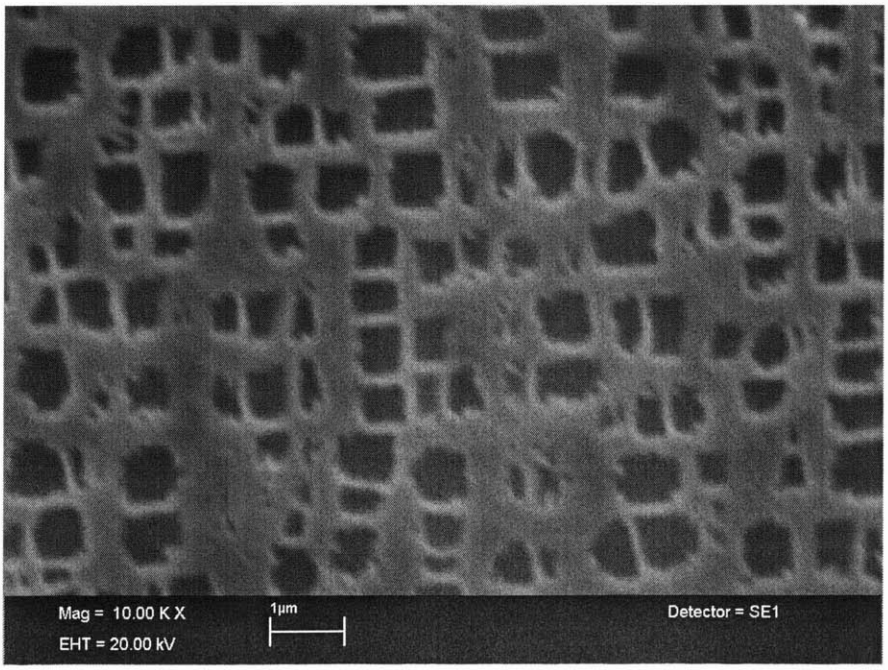

Figure 32 - After-service cubic primary γ' precipitates

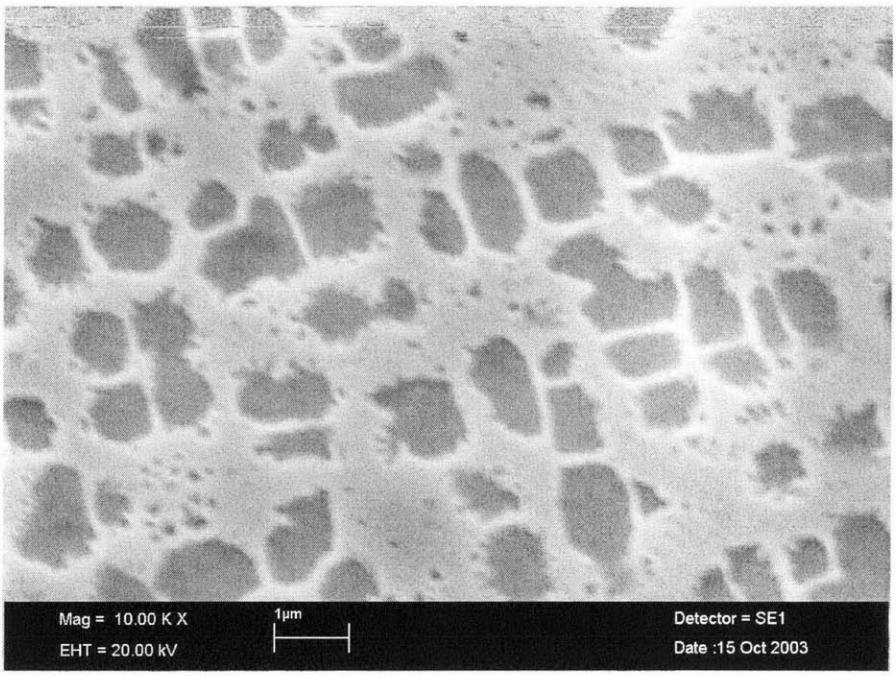

Figure 33 - S/N 083 agglomerated γ' particles in after-service condition

b. Grain boundaries microstructure morphology

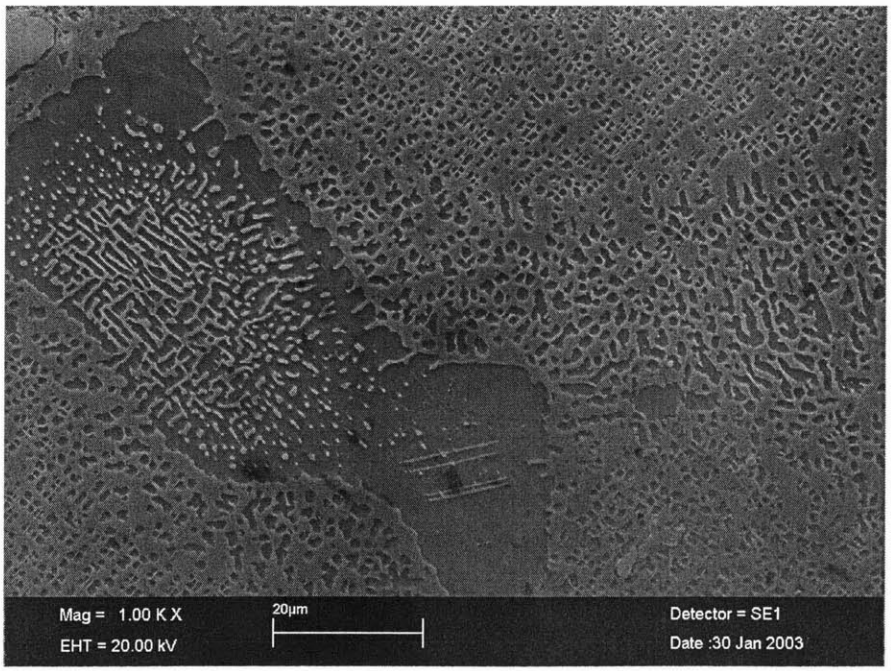

Figure 34 - TCP phase in γ' nodule at after-service material grain boundaries

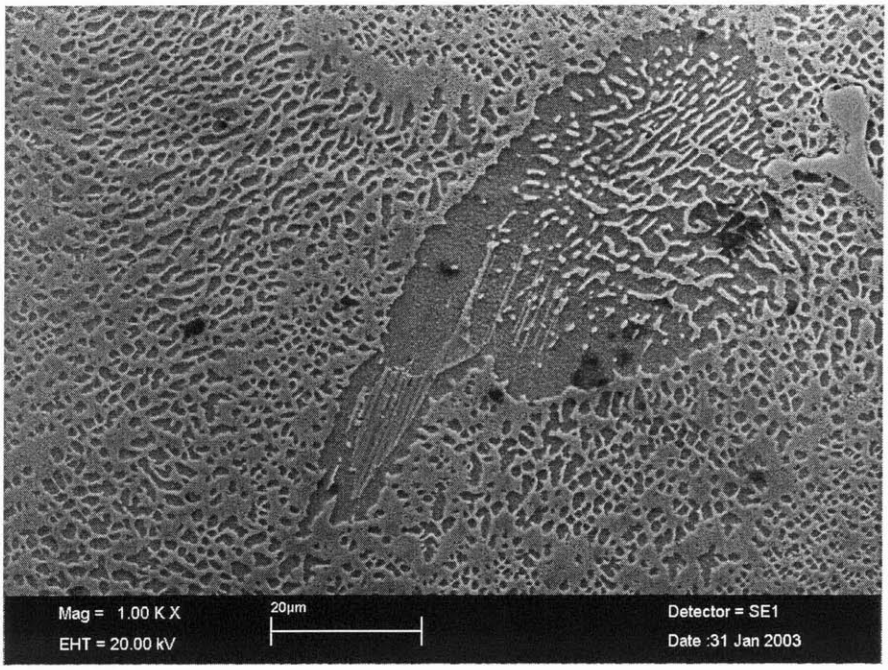

Figure 35 - Carbide & TCP phase in γ' nodule at after-service material grain boundary

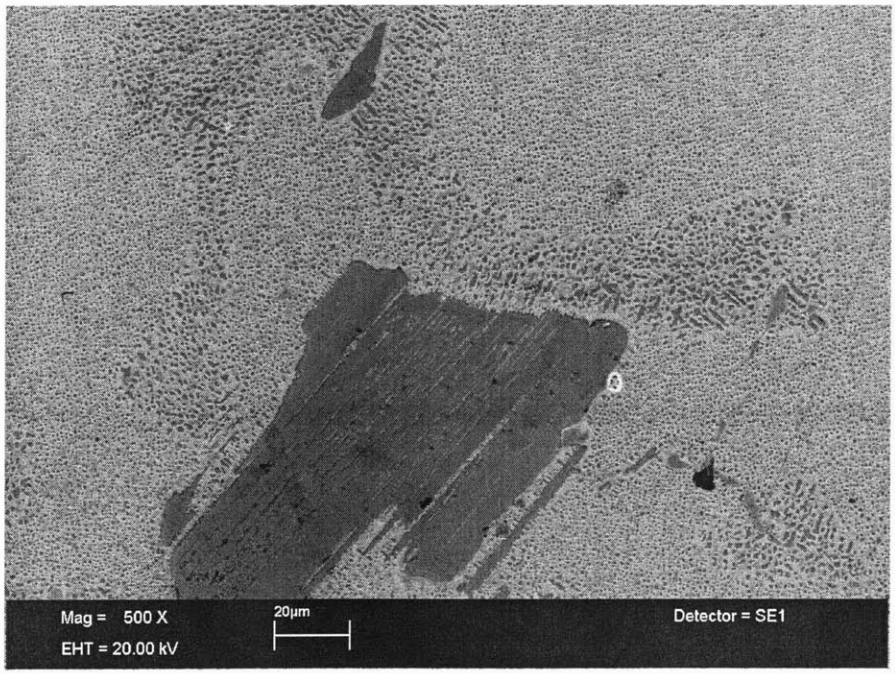

Figure 36 - After-service material grain boundary morphology

B.3 AGED

a. Primary γ' precipitates morphology

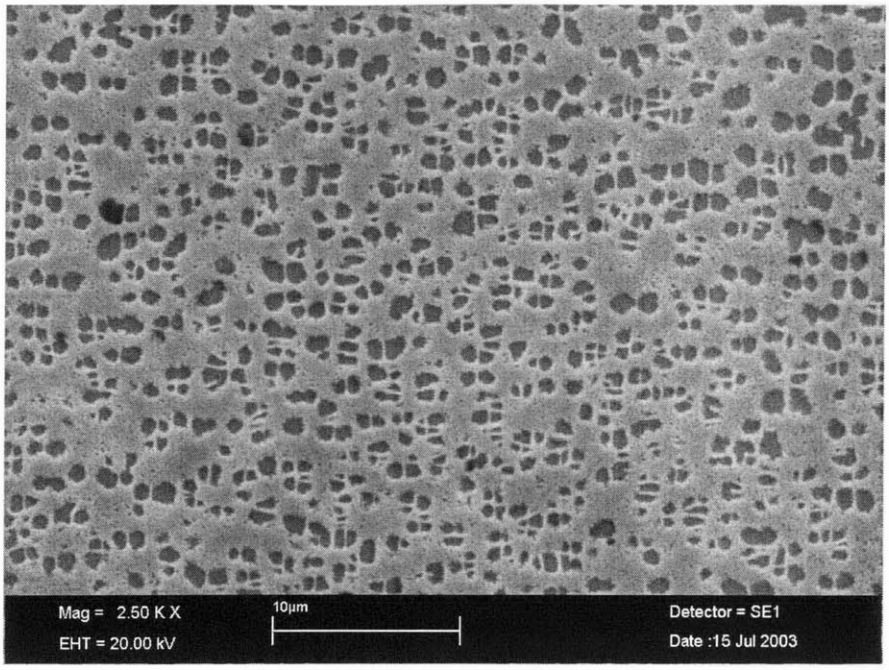

Figure 37 - Aged material γ' precipitates

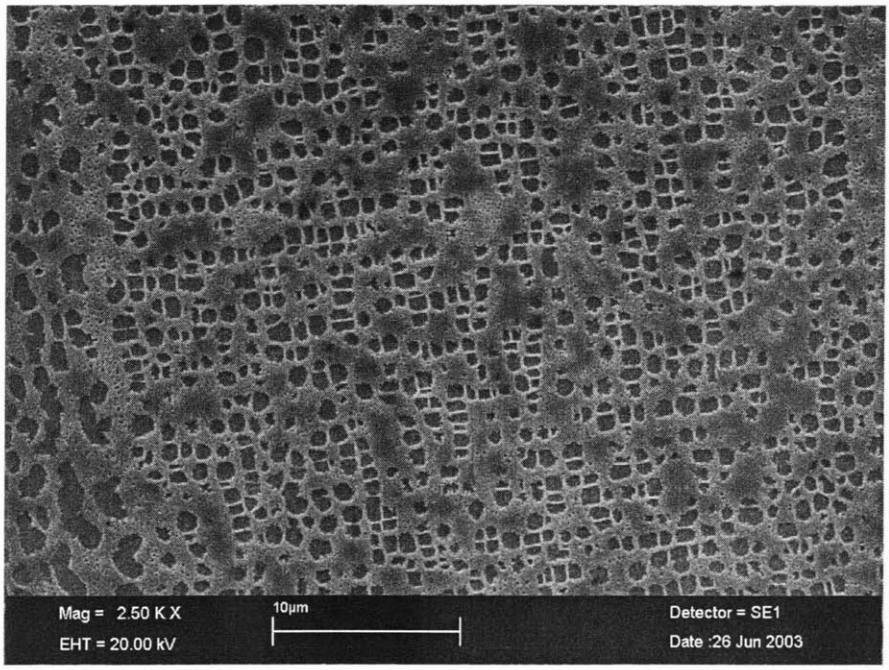

Figure 38 - Aged material primary γ' particles

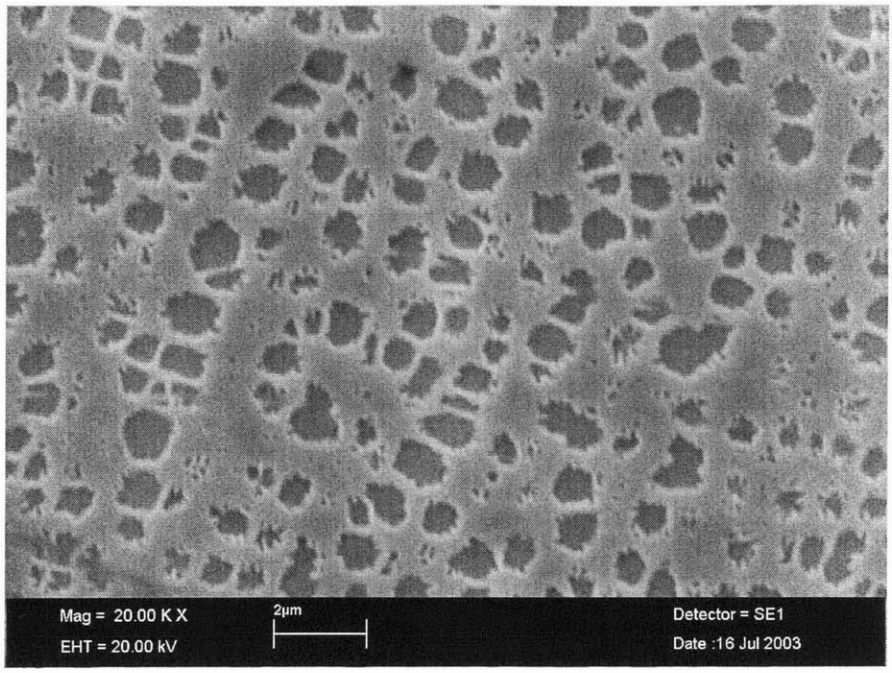

Figure 39 - Primary & secondary γ' particles in aged material

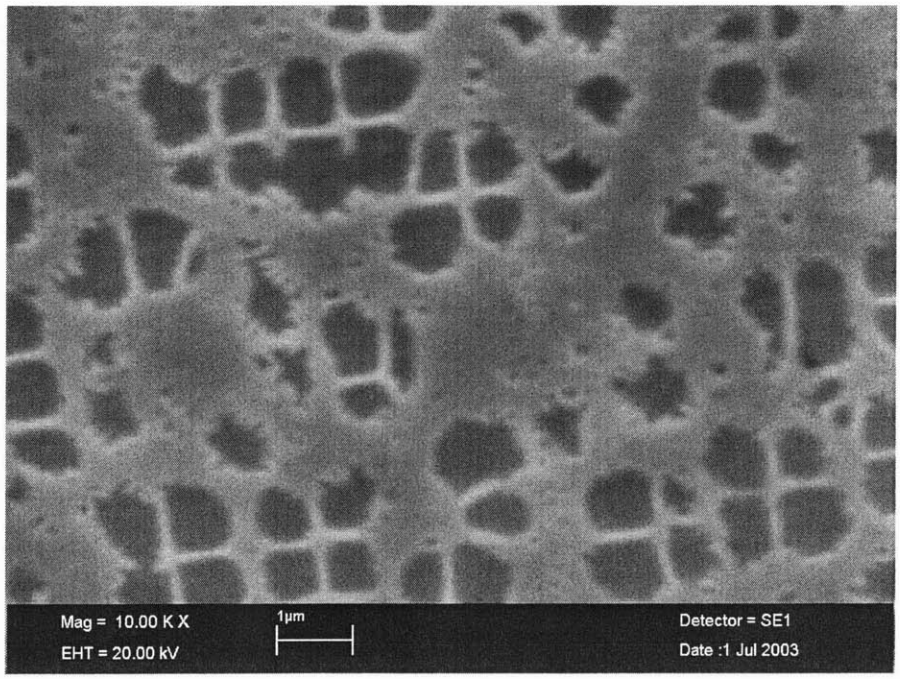

Figure 40 - Coalescing γ' particles in S/N 083 aged samples

b. Grain boundaries microstructure morphology

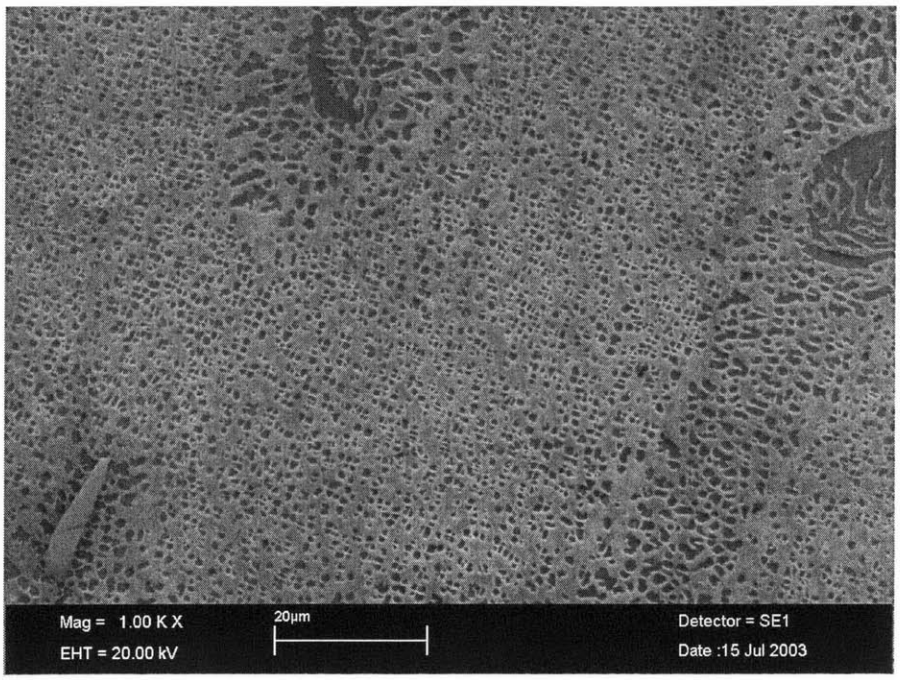

Figure 41 - Carbide & γ' nodule at aged GTD111 alloy grain boundaries

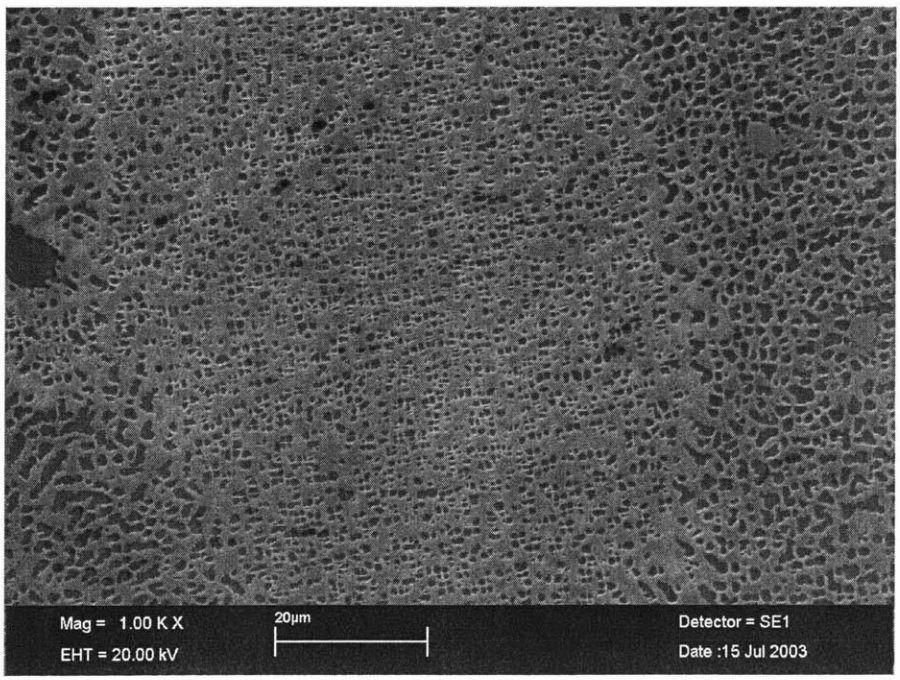

Figure 42 - Typical grain boundary morphology at aged material

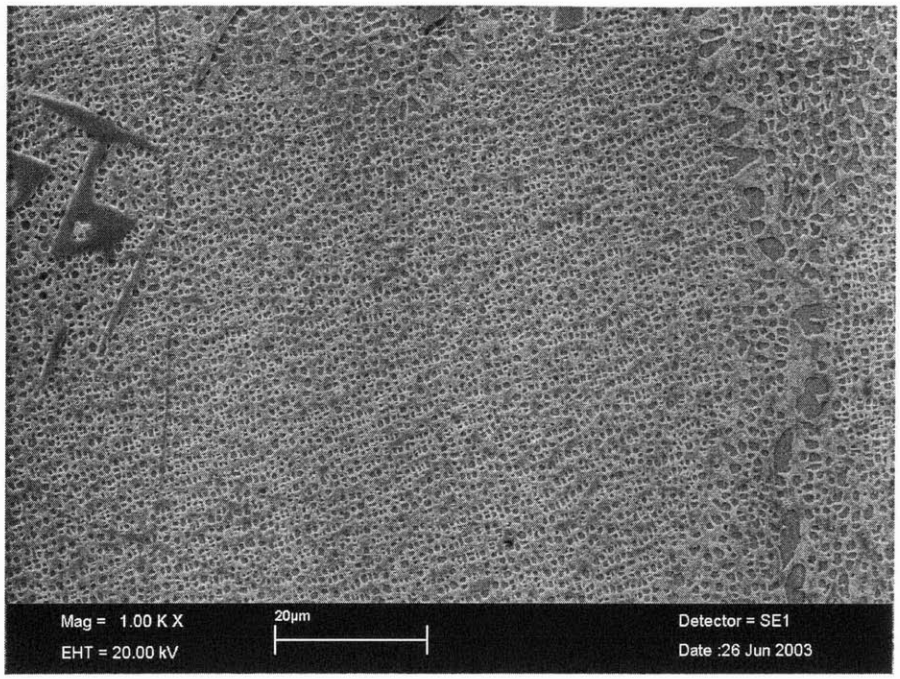

Figure 43 - γ' film & carbides in aged material grain boundaries

B.4 HIPED

a. Primary γ' precipitates morphology

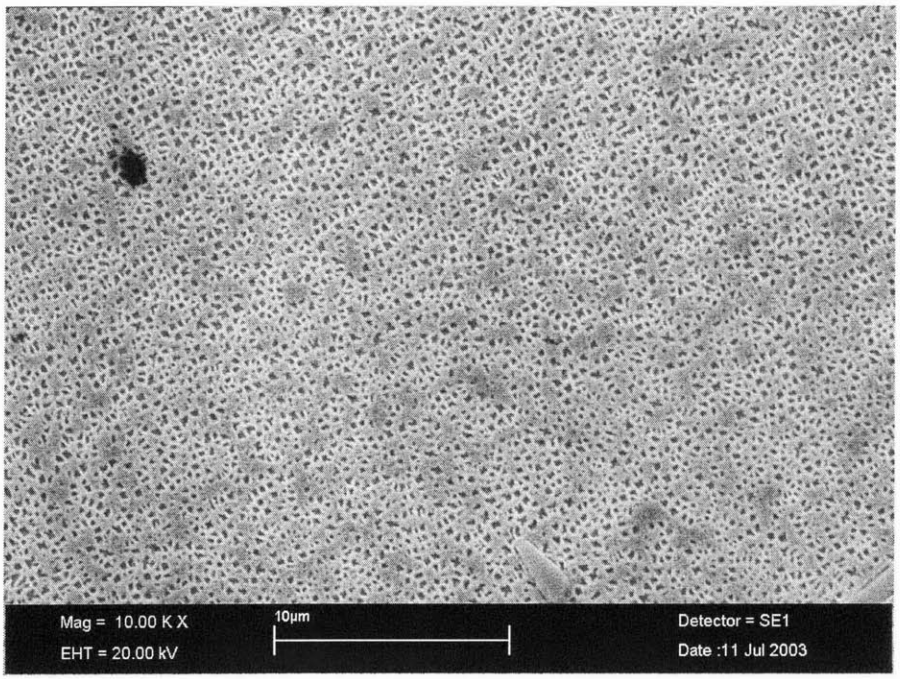

Figure 44 - Typical γ' particles morphology in HIPed condition

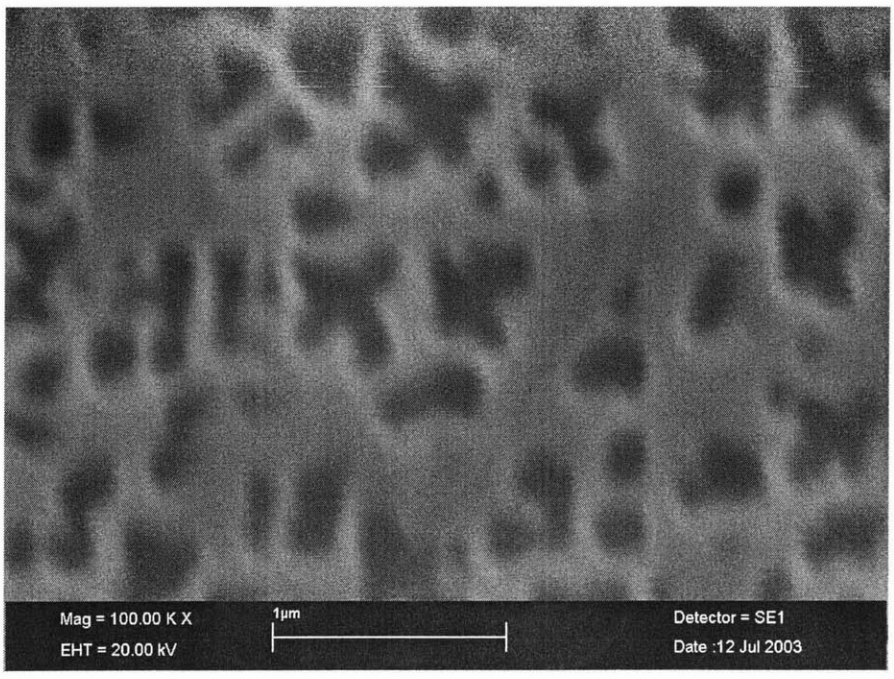

Figure 45 - Crushed cubic volume morphology of HIPed samples γ' particles

b. Grain boundaries microstructure morphology

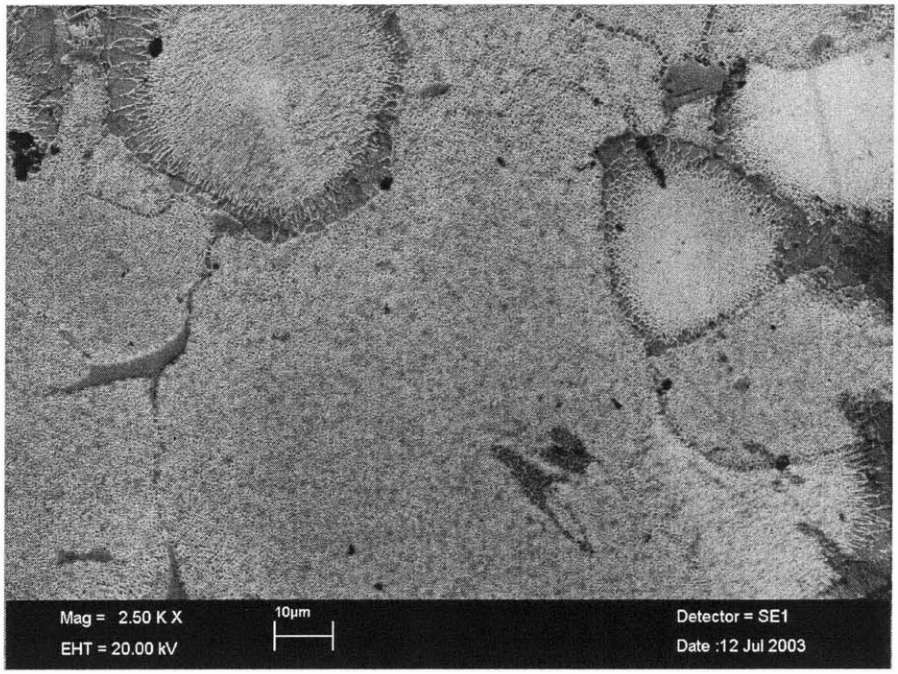

Figure 46 - Large γ-γ' nodules in GTD111 grain boundaries after HIP process

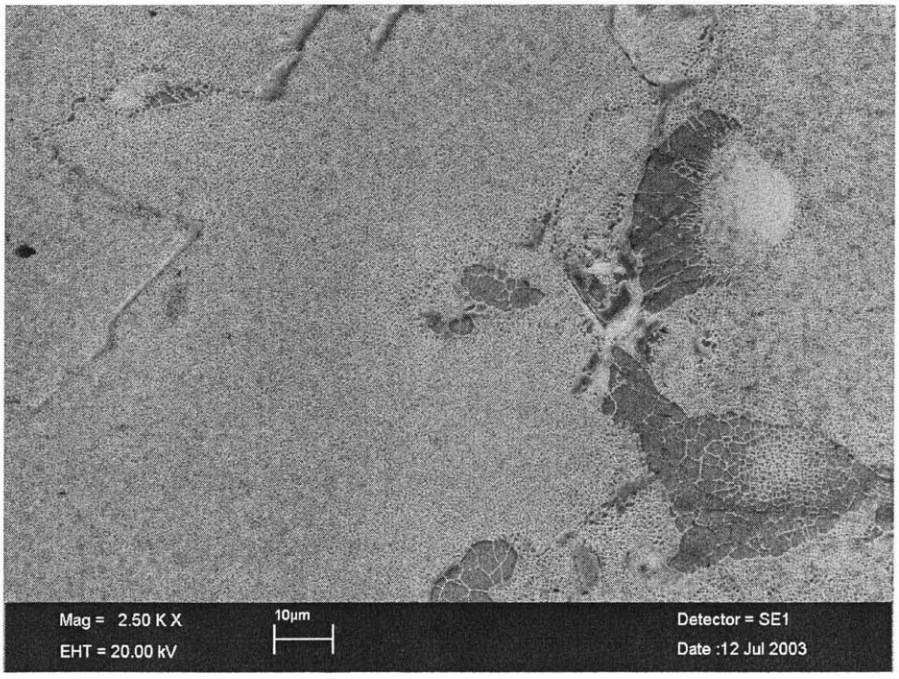

Figure 47 - Typical grain boundary morphology in HIPed GTD111 samples

B.5 HIP/SOLUTION/AGED

a. Primary γ' precipitates morphology

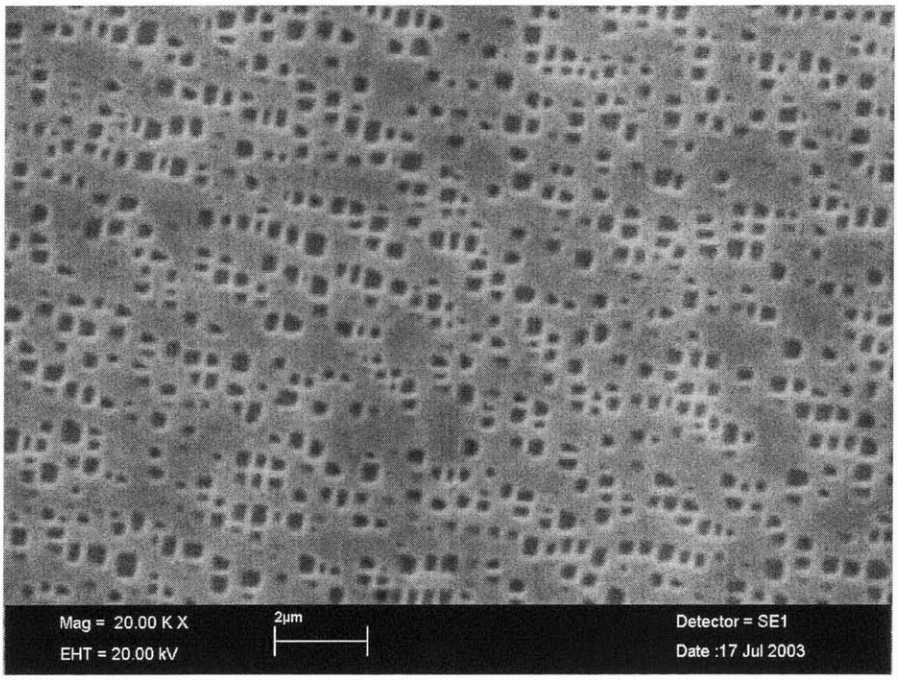

Figure 48 - γ' precipitates after HIP, high-temperature solution & aging heat treatments

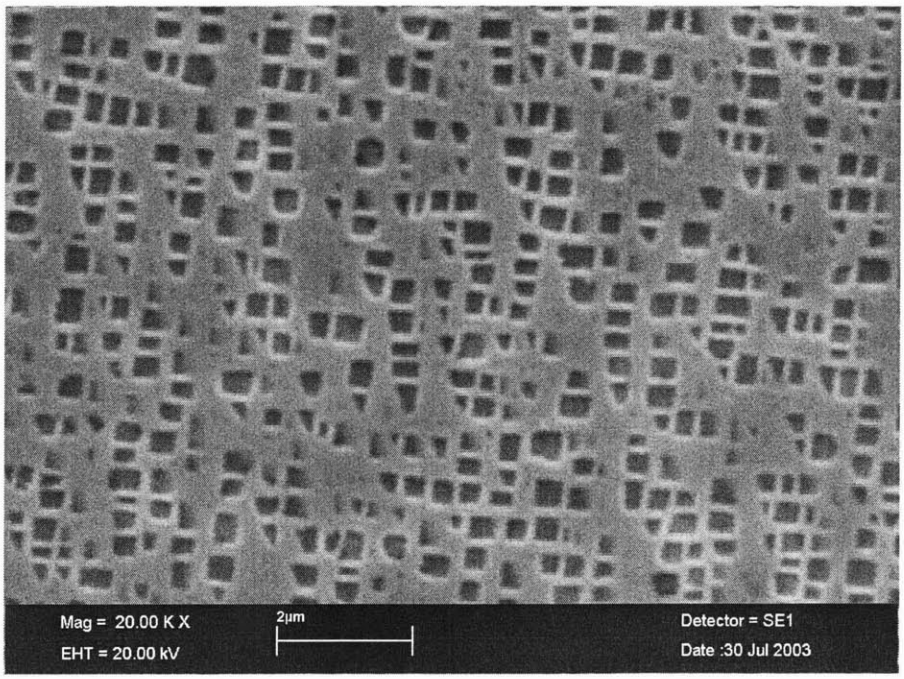

Figure 49 - Cubic γ' particles in HIP/Solution/Aged condition

b. Grain boundaries microstructure morphology

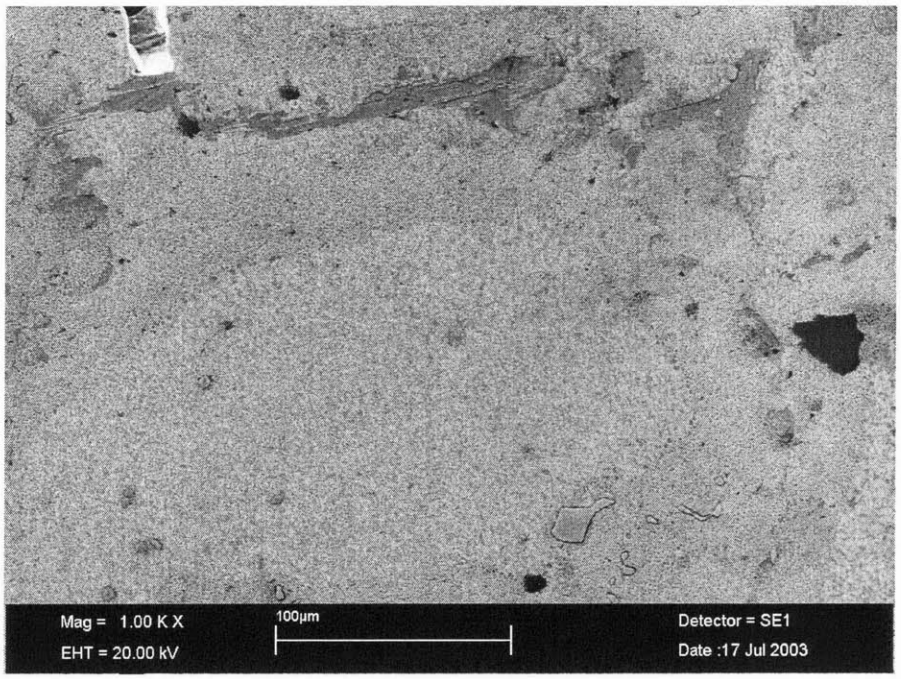

Figure 50 - Carbides & γ' film/nodules in HIP/Solution/Aged samples grain boundaries

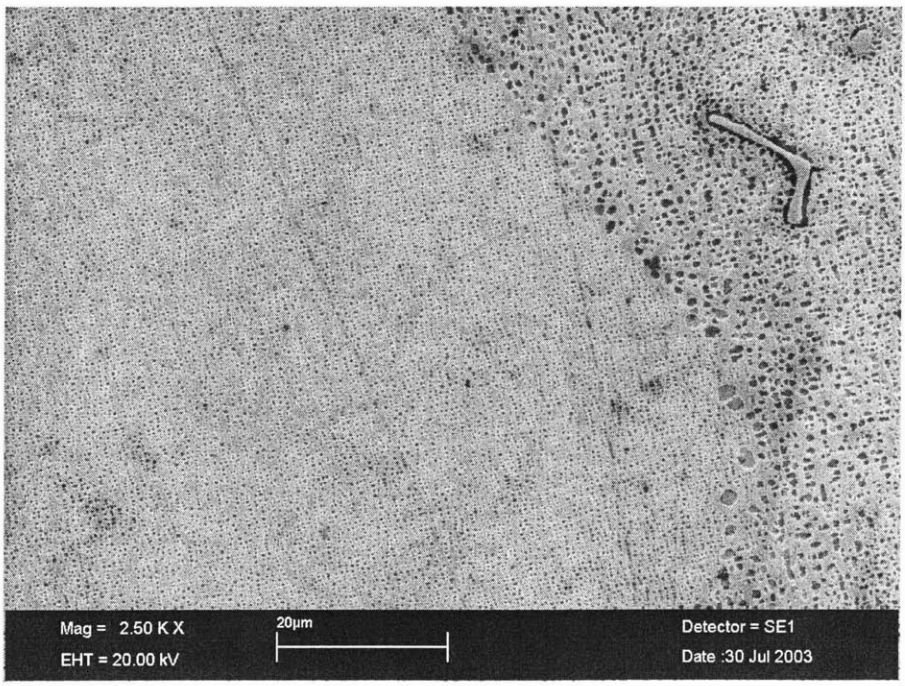

Figure 51 - Typical grain boundary morphology in HIP/Solution/Aged GTD111 alloy

Appendix C

GAMMA PRIME PARTICLE SIZE MEASUREMENTS STATISTICS

Original Condition – S/N 083

Distributions

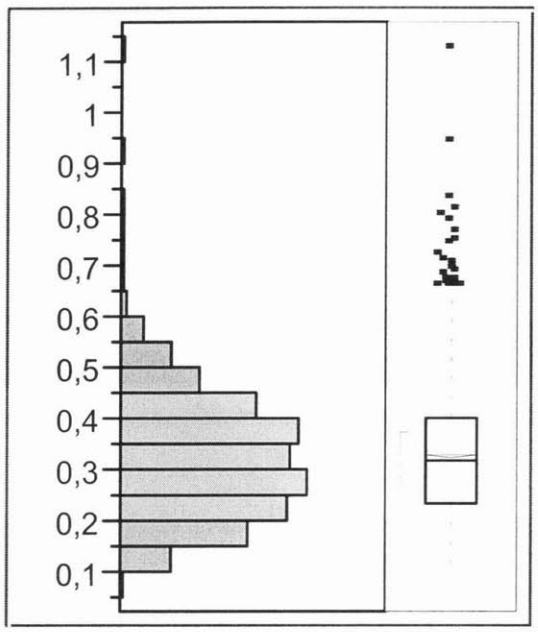

Quantiles

100.0%	maximum	1,1303
99.5%		0,6697
97.5%		0,5641
90.0%		0,4765
75.0%	quartile	0,4020
50.0%	median	0,3163
25.0%	quartile	0,2321
10.0%		0,1861
2.5%		0,1241
0.5%		0,1074
0.0%	minimum	0,0877

Moments

Mean	0,3251269
Std Dev	0,1162651
Std Err Mean	0,0018636
upper 95% Mean	0,3287808
lower 95% Mean	0,3214731
N	3892

Original Condition – S/N 849

Distributions

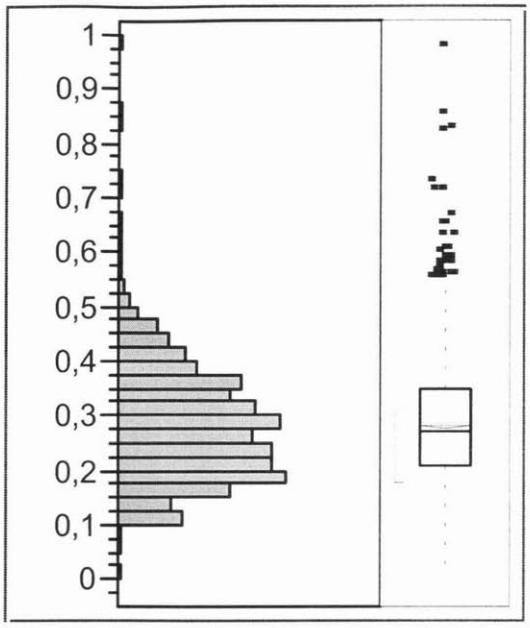

Quantiles

100.0%	maximum	0,98282
99.5%		0,55976
97.5%		0,48451
90.0%		0,41614
75.0%	quartile	0,34540
50.0%	median	0,27040
25.0%	quartile	0,20575
10.0%		0,15195
2.5%		0,12407
0.5%		0,10745
0.0%	minimum	0,00000

Moments

Mean	0,2798286
Std Dev	0,1000854
Std Err Mean	0,0013239
upper 95% Mean	0,282424
lower 95% Mean	0,2772332
N	5715

After-service Condition – S/N 083

Distributions

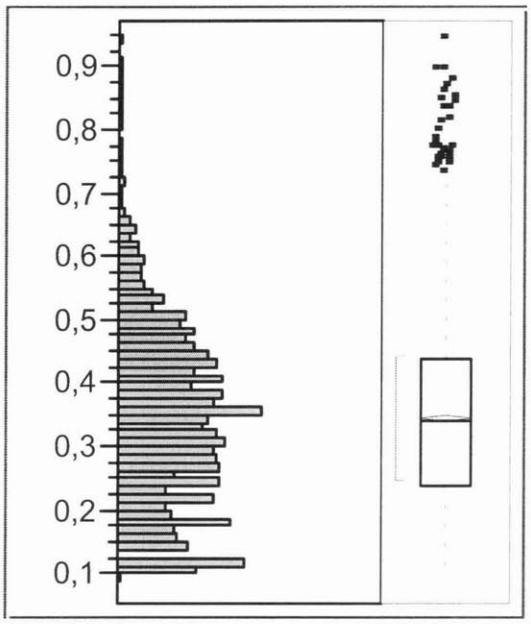

Quantiles

100.0%	maximum	0,94692
99.5%		0,78206
97.5%		0,64170
90.0%		0,53003
75.0%	quartile	0,43865
50.0%	median	0,33978
25.0%	quartile	0,24026
10.0%		0,15195
2.5%		0,10745
0.5%		0,10745
0.0%	minimum	0,08773

Moments

Mean	0,3450723
Std Dev	0,1427186
Std Err Mean	0,0024958
upper 95% Mean	0,3499658
lower 95% Mean	0,3401789
N	3270

After-service Condition – S/N 849

Distributions

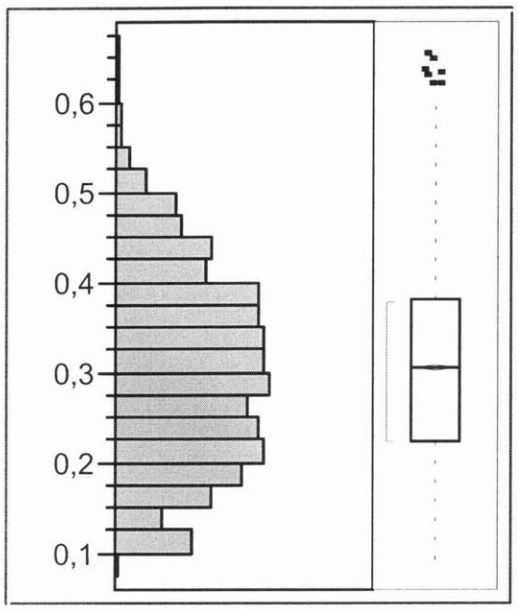

Quantiles

100.0%	maximum	0,65652
99.5%		0,58985
97.5%		0,51155
90.0%		0,45162
75.0%	quartile	0,38241
50.0%	median	0,30391
25.0%	quartile	0,22367
10.0%		0,16413
2.5%		0,12407
0.5%		0,10745
0.0%	minimum	0,08773

Moments

Mean	0,305632
Std Dev	0,1074947
Std Err Mean	0,0021254
upper 95% Mean	0,3097996
lower 95% Mean	0,3014643
N	2558

Aged Condition – S/N 083

Distributions

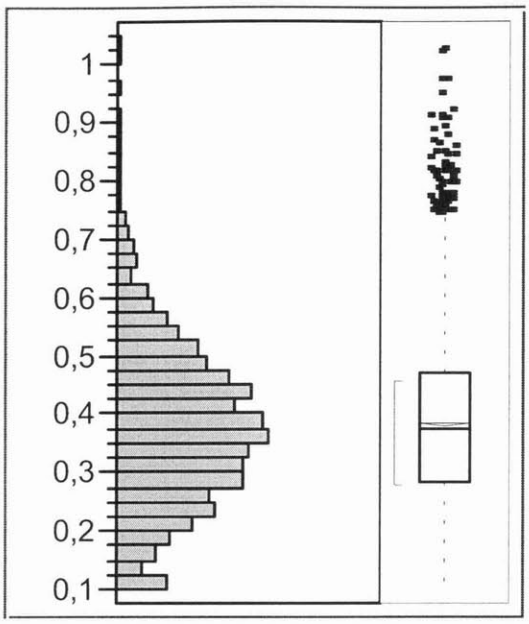

Quantiles

100.0%	maximum	1,0306
99.5%		0,8159
97.5%		0,6908
90.0%		0,5618
75.0%	quartile	0,4684
50.0%	median	0,3722
25.0%	quartile	0,2843
10.0%		0,2057
2.5%		0,1241
0.5%		0,1074
0.0%	minimum	0,1074

Moments

Mean	0,3817065
Std Dev	0,1393928
Std Err Mean	0,0018455
upper 95% Mean	0,3853244
lower 95% Mean	0,3780886
N	5705

Aged Condition – S/N 849

Distributions

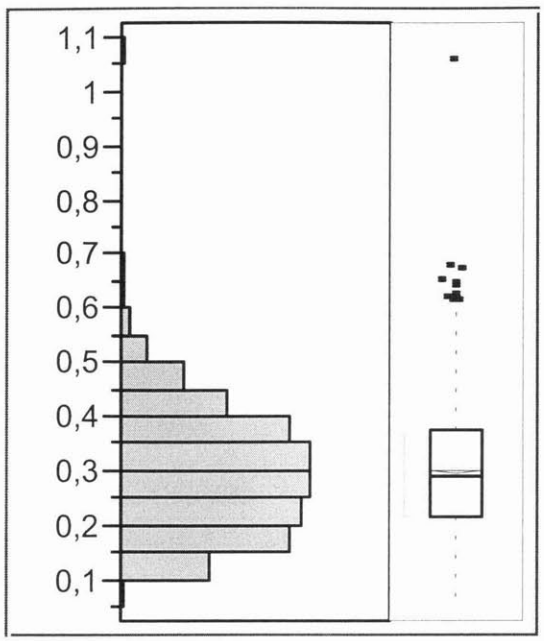

Quantiles

100.0%	maximum	1,0601
99.5%		0,5753
97.5%		0,5153
90.0%		0,4387
75.0%	quartile	0,3722
50.0%	median	0,2910
25.0%	quartile	0,2149
10.0%		0,1520
2.5%		0,1241
0.5%		0,1074
0.0%	minimum	0,0620

Moments

Mean	0,2970886
Std Dev	0,1073794
Std Err Mean	0,0017118
upper 95% Mean	0,3004447
lower 95% Mean	0,2937326
N	3935

HIPed Condition – Both buckets

Distributions

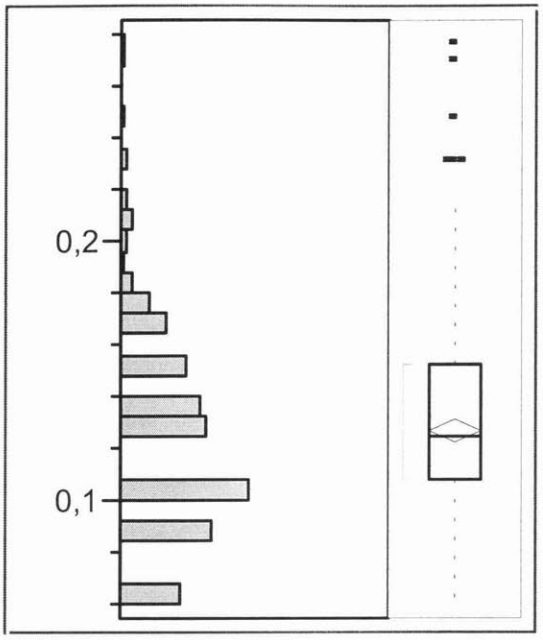

Quantiles

100.0%	maximum	0,27743
99.5%		0,27304
97.5%		0,21490
90.0%		0,17546
75.0%	quartile	0,15195
50.0%	median	0,12407
25.0%	quartile	0,10745
10.0%		0,08773
2.5%		0,06204
0.5%		0,06204
0.0%	minimum	0,06204

Moments

Mean	0,1271058
Std Dev	0,0399876
Std Err Mean	0,0022215
upper 95% Mean	0,1314763
lower 95% Mean	0,1227353
N	324

HIP/Aged Condition – Both buckets

Distributions

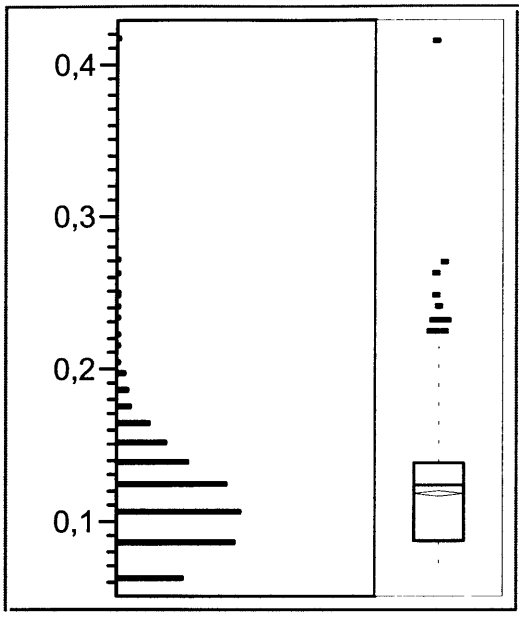

Quantiles

100.0%	maximum	0,41614
99.5%		0,22367
97.5%		0,19617
90.0%		0,16413
75.0%	quartile	0,13871
50.0%	median	0,12407
25.0%	quartile	0,08773
10.0%		0,06204
2.5%		0,06204
0.5%		0,06204
0.0%	minimum	0,06204

Moments

Mean	0,1182313
Std Dev	0,035009
Std Err Mean	0,0005906
upper 95% Mean	0,1193893
lower 95% Mean	0,1170734
N	3514

HIP/Solution/Aged Condition – Both buckets

Distributions

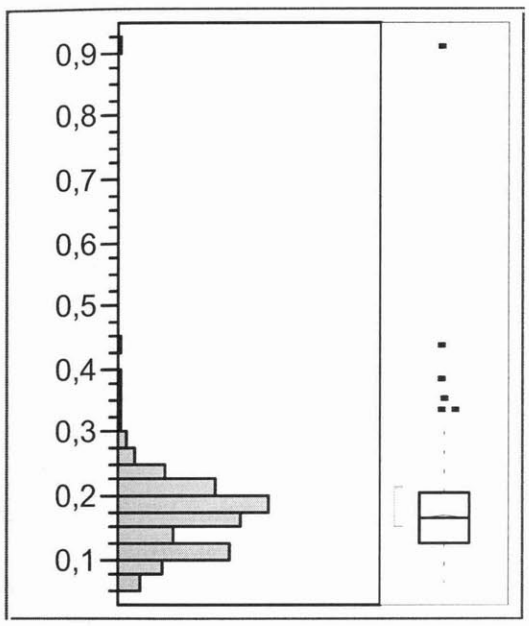

Quantiles

100.0%	maximum	0,90961
99.5%		0,29751
97.5%		0,26319
90.0%		0,23211
75.0%	quartile	0,20575
50.0%	median	0,16413
25.0%	quartile	0,12407
10.0%		0,08773
2.5%		0,06204
0.5%		0,06204
0.0%	minimum	0,06204

Moments

Mean	0,1666538
Std Dev	0,0524486
Std Err Mean	0,0008506
upper 95% Mean	0,1683215
lower 95% Mean	0,1649861
N	3802

Bibliography

1. Eldrid, R., Kaufman, L., Marks, P., *The 7FB: The Next Evolution of the F Gas Turbine*. Apr 2001, GE Power Systems: Schenectady, NY.
2. *General Electric Model 7000*. 1995, Forecast-International.
3. Schilke, P.W., Foster, A.D., Pepe, J.J., Beltran, A.M., *Advanced Materials Propel Progress in Land-Based Gas Turbines*. Advanced Materials & Processes, 1992(4/92): p. 22-30.
4. Hale, J.M., *Procedure Development for the Repair of GTD-111 Gas Turbine Bucket Material*. ASME COGEN-TURBO, 1994. **IGTI-Vol.9**: p. 63-76.
5. DeHoff, R.T., Rhines, F.N., *Quantitative Microscopy*. 1968: McGraw-Hill.
6. Daleo, J.A., Wilson, J.R., *GTD111 Alloy Material Study*. Journal of Engineering for Gas Turbines and Power, 1998. **120**(April 1998): p. 375-382.
7. Sims, C.T., Stoloff, N.S., Hagel, W.C., *Superalloys II*. 1987: Wiley-Interscience.
8. Cheruvu, N.S., Swaminathan, V.P. *Recovery of microstructure and mechanical properties of service run GTD-111 DS buckets*. in *International Gas Turbine & Aeroengine Congress & Exhibition*. 1999. Indianapolis, Indiana: AMSE.
9. Swaminathan, V.P., Cheruvu, N.S. *Microstructure and property assessment of conventionally cast and directionally solidified buckets refurbished after long-term service*. in *International Gas Turbine & Aeroengine Congress & Exhibition*. 1998. Stockholm, Sweden: ASME.
10. Swaminathan, V.P., Lowden, P., *Gas turbine blade life assessment and repair guide*. 1989.
11. Durand-Charre, M., *The microstructure of superalloys*. 1997, Amsterdam, The Netherlands: Gordon & Breach Science Publishers.
12. Prikodko, S.V., Ardell A.J., *Coarsening of gamma prime in Ni-Al alloys aged under uniaxial compression: III. Characterization of the morphology*. Acta Mater, 2003. **51**(2003): p. 5021-5036.
13. Chellman, D.J., Ardell, A.J., *The coarsening of gamma prime precipitates at large volume fractions*. Acta Metallurgica, 1974. **22**(May 1974): p. 577-588.
14. Stevens, R.A., Flewitt, P.E, *The effects of gamma prime precipitate coarsening during isothermal aging and creep of the Nickel-base superalloy IN-738*. Materials Science and Engineering, 1979. **37 (1979)**: p. 237-247.
15. Boyce, M.P., *Gas turbine engineering handbook*. 2001: Gulf Professional Publishing.
16. Ted Pella, I., http://www.tedpella.com/calibrat_html/caSEMmag.htm.